The role of thermokarst evolution in debris flow initiation (Hüttekar Rock Glacier, Austrian Alps)

Simon Kainz[1], Thomas Wagner[1], Karl Krainer[2], Michael Avian[3], Marc Olefs[3], Klaus Haslinger[3], and Gerfried Winkler[1]

[1]Institute of Earth Sciences, NAWI Graz Geocenter, University of Graz, Heinrichstrasse 26, 8010 Graz, Austria
[2]Institute of Geology, University of Innsbruck, Innrain 52, 6020 Innsbruck, Austria
[3]Department of Climate Impact Research, GeoSphere Austria, Hohe Warte 38, 1190 Vienna, Austria

Correspondence: Simon Kainz (simon.kainz@uni-graz.at)

Abstract. A rapid sequence of cascading events involving thermokarst lake outburst, local rock glacier front failure, debris flow development, and river blockage hit Radurschl Valley (Ötztal Alps, Tyrol) on 13 August 2019. Compounding effects from multivariate permafrost degradation and drainage network development within the rock glacier initiated the complex process chain. The debris flow dammed the main river of the valley, impounding a water volume of 120,000 m^3 that was partly drained by excavation to prevent a potentially catastrophic outburst flood. Since the environmental forces inducing the debris flow evolved under ambiguous conditions, potentially destabilizing factors were analyzed systematically We present a systematic analysis of destabilizing factors to deduce the failure mechanismand establish a basis for multi hazard assessment in similar settings. Identification and evaluation of individual factors revealed reveals a critical combination of topographical and sedimentological disposition, climate, and weather patterns driving the evolution of thermokarst and debris flowa thermokarst drainage network. Progressively changing groundwater flow and storage patterns characterizing the hydraulic configuration within the frozen sediment accumulation governed the slope stability of the rock glacier front. The Our results demonstrate the hazard potential of active rock glaciers due to their large amount of mobilizable sediment, dynamically changing internal structure, thermokarst lake development, and substantial water flow along a rapidly evolving channel networkeroded into the permafrost body, render active rock glaciers complex multi hazard elements in periglacial, mountainous environments.

1 Introduction

Climate change and its adverse effects on slope stability rapidly alter patterns of landslide occurrence and the balance between destabilizing and resisting forces (Crozier, 2010; Gariano and Guzzetti, 2016; Adler et al., 2022)(Gariano and Guzzetti, 2016; Adler et al., 2022). Landslide engineers and decision makers face a delicate challenge since data-driven hazard assessment methods are at risk of losing predictive power as boundary conditions change at timescales that are short compared to typically available landslide records (Haeberli and Whiteman, 2015; Patton et al., 2019). In this context, a process-based understanding of potential failure mechanisms is indispensable for identifying landslide hazard at sites considered stable under past conditions (Evans and Delaney, 2015; Schauwecker et al., 2019). This is especially true for debris flows initiating in permafrost affected terrain, due to the rapid alteration of slope stability in their initiation zones, their ability to traverse great distances at high velocities, and their high impact forces (Jakob and Hungr, 2005; Jakob et al., 2012; Petley, 2012; Dowling and Santi, 2014; Nikolopoulos et al., 2014)(Petley, 2012; Dowling and Santi, 2014). Hence failure in remote areas which are typically characterized by data scarcity and incomplete monitoring has the potential to dramatically affect people and infrastructure far from debris flow initiation (Haque et al., 2016, 2019).

The European Alps are affected by severe increases in surface air temperature (∼0.3 °C per decade, exceeding global warming rates), altering snow cover dynamics and driving permafrost thaw (Beniston et al., 2018; Hock et al., 2019; Patton et al., 2019; Olefs et al., 2020; Matiu et al., 2021; Fox-Kemper et al., 2021)(Beniston et al., 2018; Olefs et al., 2020; Fox-Kemper et al., 2021). The increasing frequency of high-intensity precipitation events amplifies the likelihood of landslides (Giorgi et al., 2016; Rajczak and Schär, 2017; Schlögl and Matulla, 2018; Hock et al., 2019; Patton et al., 2019; Ranasinghe et al., 2021)(Ranasinghe et al., 2021). Slope stability decreases as subsurface liquid water content, ice ductility, and permeability increase in response to permafrost degradation (Patton et al., 2019; Hock et al., 2019). Moreover, glacier retreat enhances the accumulation of loose, unstable sediment at high elevations (Stoffel and Huggel, 2012; Deline et al., 2015; Buckel et al., 2018; Hock et al., 2019; Mölg et al., 2021)(Deline et al., 2015; Hock et al., 2019). These changing environmental conditions alter the geotechnical and hydraulic ground properties, and modify the characteristics and seasonality of landslides accordingly (Stoffel and Huggel, 2012; Gariano and Guzzetti, 2016; Beniston et al., 2018; Patton et al., 2019)(Stoffel and Huggel, 2012; Gariano and Guzzetti, 2016; Patton et al., 2019). The consecutive variation in process chains and cascading events makes them especially difficult to predict under a changing climate, with potentially catastrophic consequences downstream (Deline et al., 2015).

In terms of landslide initiation, the steep slopes and The large sediment accumulations provided by active rock glacier fronts pose a serious hazard. Active rock glaciers, i. e. distinct sediment accumulations consisting of ice-debris mixtures accumulations slowly creeping downhill, constitute important periglacial landforms regarding sediment dynamics and hydrology due to their large sediment transfer capability, pronounced water storage capacity, and wide-spread occurrence in mountainous terrain (Kummert and Delaloye, 2018; Winkler et al., 2018; Jones et al., 2019b; Hayashi, 2020; Wagner et al., 2020, 2021a). Common deformation rates are on the order of decimeters to meters per year, accelerating across the European Alps in response to climate change (Kääb et al., 2007; Roer et al., 2008; Beniston et al., 2018; Groh and Blöthe, 2019; Hock et al., 2019; Kenner et al., 2020; Fleischer et al., 2021; Fox-Kemper et al., 2021; Marcer et al., 2021)pose a serious hazard in terms of landslide initiation. Thermo–hydro–mechanical processes determine the deformation characteristics of rock glaciers, with plastic deformation governed by permafrost ice content and temperature, while discrete shear failure is commonly initiated by elevated pore-water pressures along the failure surface (Arenson and Springman, 2005; Ikeda et al., 2008; Buchli et al., 2013, 2018; Krainer et al., 2015; Cicoira et al., 2019; Kofler et al., 2021). Active rock glaciers exhibit complex drainage patterns indicating a dual groundwater flow system, where large amounts of water are rapidly transported along a network of convoluted meltwater channels eroded into the frozen rock glacier core (Wahrhaftig and Cox, 1959; Potter, 1972; White, 1971; Johnson, 1978; Giardino et al., 1991; Burger et al., 1999; Krainer and Mostler, 2002; Vonder Mühll et al., 2003; Arenson et al., 2010; Springman et al., 2012; Winkler et al., 2018; Jones et al., 2019b; Wagner et al., 2021b; Kainz, 2022)(Arenson and Springman, 2005; Krainer et al., 2015; Kofler et al., 2021). Common deformation rates are on the order of decimeters to meters per year, accelerating across the European Alps in response to climate change (Hock et al., 2019; Marcer et al., 2021). Previous research demonstrated that hydrological processes fundamentally control the style and rate of rock glacier kinematics (Ikeda et al., 2008; Buchli et al., 2013, 2018; Cicoira et al., 2019). However, while the impact of thermokarst evolution on the storage and release of water in these landforms is well documented, its role in debris flow initiation at rock glacier fronts remains largely unknown (Krainer and Mostler, 2002; Winkler et al., 2018; Jones et al., 2019b; Kainz, 2022).

Active rock glaciers constitute multi hazard elements (Kappes et al., 2012; Gallina et al., 2016) in that they induce a spectrum of mass movement processes ranging from occasional rockfall to debris flow events, potentially involving complex chain processes (Burger et al., 1999; Kummert and Delaloye, 2018; Kummert et al., 2018). Destabilizing rock glaciers frequently experience significant acceleration, often accompanied by the appearance of morphological discontinuities such as cracks and crevasses (Kääb et al., 2007; Roer et al., 2008; Stoffel and Huggel, 2012; Delaloye et al., 2013; Marcer et al., 2019). Debris flows initiated by destabilizing rock glacier fronts occur most frequently in response to heavy rainfall (e.g., Krainer et al. (2012); Marcer et al. (2020); Kofler et al. (2021)). However, intense snowmelt, rain-on-snow events, and exceptionally warm periods have also been discerned as triggering factors (Rebetez et al., 1997; Lugon and Stoffel, 2010; Krainer et al., 2012; Bodin et al., 2017; Kummert et al., 2018; Marcer et al., 2020; Kofler et al., 2021)(Lugon and Stoffel, 2010; Bodin et al., 2017; Kummert et al., 2018). Regardless of the detailed initiation process, the mechanics of debris flows require excessive amounts of water, capable of transporting the mobilized debris down the flow path (Soeters and van Westen, 1996). Thus, assessing the hazard potential of rock glaciers requires an integrated approach combining hydrogeological, meteorological, thermal, geomorphological, and mechanical aspects in a coherent framework.

The aim of this paper is to explore the destabilizing factors leading to local failure of an active rock glacier front in a the high mountain cirque , and the actuated Hüttekar in the Austrian Alps. We analyze the cascading processes involving thermokarst lake outburstflood, debris flow, and river blockage. We evaluate By evaluating a set of potentially contributing factors , assess critical combinations, and and assessing critical factor combinations, we develop a consistent conception explaining debris flow initiation and evolutionat the rock glacier front. Similarities and differences with respect to documented rock glacier front failures and glacial lake outburst floods (GLOFs) debris flows at other rock glacier fronts are analyzed, and conclusions drawn regarding hazard potential.

2 Study site

The study site comprises the highest areas of Radurschl Valley, a valley in the Western Ötztal Alps constituting a headwater tributary to the Inn River (Fig. 1). The landscape is characterized by rugged terrain of glacial and periglacial origin, including steep slopes and crests, interrupted by relatively flat areas domains covered by talus, moraines, and periglacial sediments. The area shows an exceptionally high rock glacier density (56 % areal coverage), as well as small remnants of cirque glaciers in its uppermost parts(Kerschner, 1982; Krainer and Ribis, 2012; Wagner et al., 2020, 2021a).

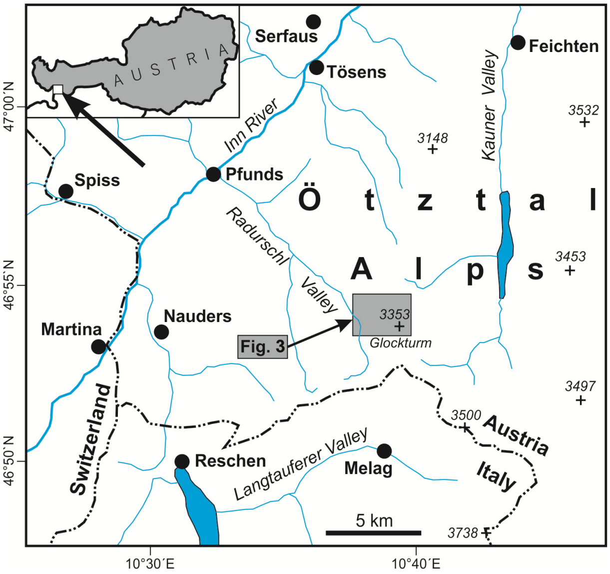

Figure 1. Location map of Hüttekar Hüttekar-cirque in the Ötztal Alps, Tyrol (Austria).

The specific cirque under consideration is the Hüttekar-cirque, a small (2.8 km^2) headwater catchment encircled by ragged rock walls except to the west, where it steeply descends to Radurschl Valley (Fig. 2; 46°54´ N, 10°39´ E). The altitudinal range in the study area varies Its altitude ranges from 2,387 to 3,353 m a. s. l.(mean altitude 2,870 m a. s. l.), including a relatively flat valley bottom between 2,600 and 2,700 m a. s. l. The bedrock lithology is composed of metamorphic rocks of the Ötztal–Stubai–Complex (Ötztal–Bundschuh nappe system; Hoinkes and Thöni (1993); Schmid et al. (2004)),as illustrated in Fig. 3. The mountain ridges bordering the cirque to the south and to the east are dominated by orthogneiss (augen- and flasergneiss), the ridge to the north and northwest exhibits muscovite-granite-orthogneiss. At Rotschragenjoch and south of Bruchkopf, paragneiss and micaschist with thin intercalations of amphibolite are exposed(mean catchment altitude 2,870 m a. s. l.). The terrain is composed of bedrock (38 %), mainly exposed in the highest parts, talus, . Talus and debris slopes (17 %) dominate along the valley sides, while the lower parts are covered by moraine deposits (12 %) and four rock glaciers (27 %). Two small, north facing cirque glaciers (Glockturmferner, Hüttekarferner; 6 %) are situated at mean altitudes of 2,853 and 3,029 m a. s. l., respectively (Fig. 3).

The bedrock lithology is composed of metamorphic rocks of the Ötztal–Stubai–Complex (Ötztal–Bundschuh nappe system; Hoinkes and Thöni (1993); Schmid et al. (2004)). The mountain ridges bordering the cirque to the south and to the east are dominated by orthogneiss (augen- and flasergneiss), the ridge to the north and northwest exhibits muscovite-granite-orthogneiss (Fig. 3). At Rotschragenjoch and south of Bruchkopf, paragneiss and micaschist with thin intercalations of amphibolite are exposed.

The local climate is influenced by the dry, inner alpine conditions prevailing in the Ötztal Alps (Frei and Schär, 1998; Isotta et al., 2014). Moderate annual precipitation (Isotta et al., 2014). With respect to long-term (1976-2019) averages across

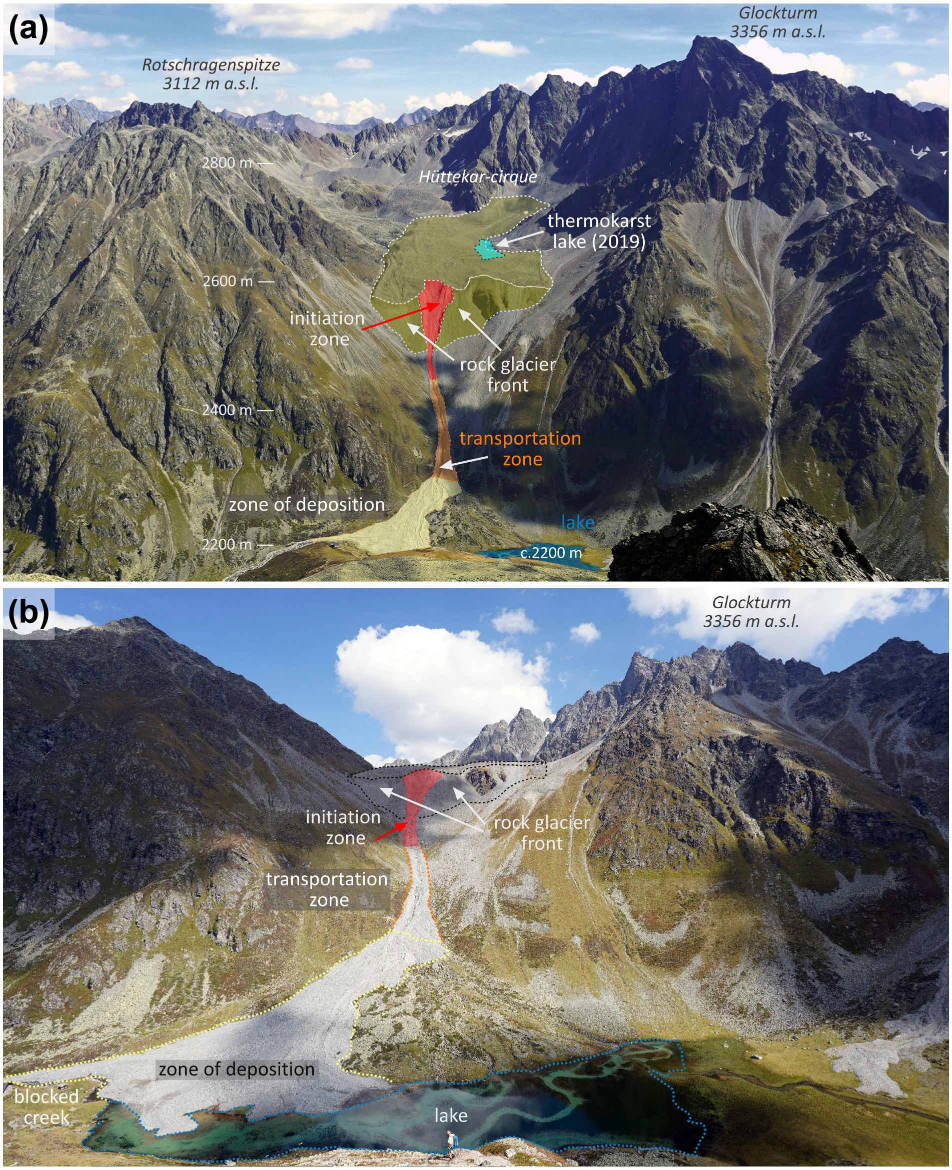

Figure 2. (a) Illustration of Hüttekar-cirque, Hüttekar Rock Glacier, the debris flow and the impounded lake (view is towards the east). The debris flow was initiated at the steep front of Hüttekar Rock Glacier (highlighted), caused by rapid drainage of a thermokarst lake that existed between 01 June and 13 August 2019 (former position indicated). The debris flow path sections are outlined and labelled according to Hungr (2005). (b) Debris flow morphology two years after its initiation. The progressively enlarging initiation zone eroded already significant parts of the steep rock glacier front. The transport zone is characterized by a set of levees along a narrow channel. The former flow path of the blocked river is still clearly visible below the lake surface. The channel draining the lake was excavated to prevent a potentially catastrophic outburst following river blockage in August 2019 (photographs: Rudolf Philippitsch, 14 September 2021).

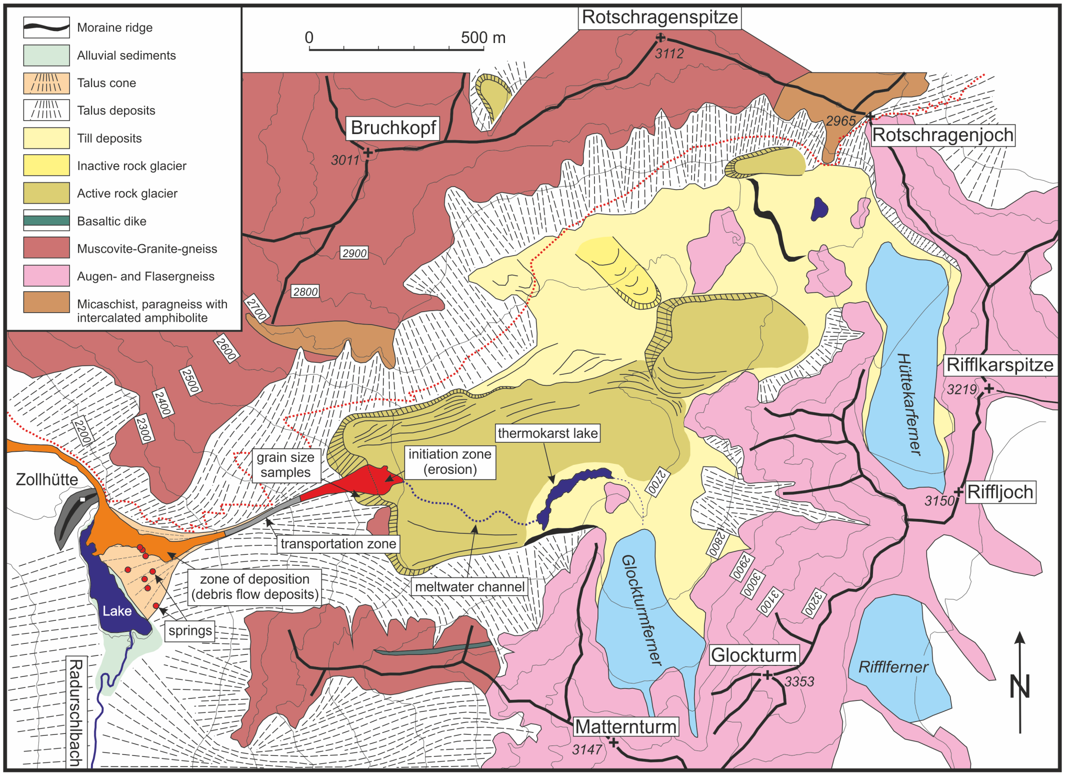

Figure 3. Geological-geomorphological map, compiled using the most recent provisional geological map provided by the Geological Survey of Austria (Moser, 2012). It is complemented by ortho-images and a high-resolution digital terrain model (DTM) derived from airborne laser scanning data (Government of the Province of Tyrol, 2021a). The preliminary map is based on comprehensive field mapping (2019–2021).Numbers indicate grain size analysis sampling locations.

Austria, annual precipitation is moderate (1042 mm) and low mean annual air temperature is low (-2.5°C)reflect , reflecting the high altitude of Hüttekar-cirque and its central position close to the main chain of the Alps (corresponding areal averages across Austria are 1077 mm and 6.6°C, respectively). Monthly precipitation reaches its maximum in August and its minimum in February, with the respective months corresponding to the highest and lowest mean air temperature (Table 1). The local altitude distribution and dry climatic conditions and the local elevation distribution promote the development of rock glaciers. The equilibrium line altitude of glaciers, rising from ∼3,100 to ∼3,300 m a. s. l. during the 20th century, is located within the steep summit region (Žebre et al., 2021). These unfavorable conditions for cirque glacier development allow rock glaciers to cover the extensive flat terrain above the lower permafrost boundary, ranging from ∼2,400 to ∼2,600 m a. s. l. (Kerschner, 1982; Boeckli et al., 2012a; Ribis, 2017)(Kerschner, 1982; Ribis, 2017).

The coevolution of cirque glaciers and rock glaciers is highlighted by comparing a set of glacier inventories ranging from the little ice age (about 1850 CE) to 2015 CE largest rock glacier in this cirque, Hüttekar Rock Glacier, is 1408 m long and up to 493 m wide, covering an area of 0.5 km in the lowermost parts of the cirque (Fig. 3, Supplementary Fig. S1; Fischer et al.

Table 1. Long-term (1976–2019) mean monthly air temperature and precipitation in Hüttekar-cirque(. Values are calculated based on Hiebl and Frei (2016, 2018)the continuously updated SPARTACUS dataset (Spatiotemporal Reanalysis Dataset for Climate in Austria), as described in Hiebl and Frei (2016, 2018).

	J	**F**	**M**	**A**	**M**	**J**	**J**	**A**	**S**	**O**	**N**	**D**
Air temperature (°C)	-9.7	-9.8	-7.7	-4.9	-0.3	3.2	5.4	5.4	2.3	-0.5	-5.5	-8.4
Precipitation (mm)	64	45	61	57	99	125	151	156	90	71	61	62

(2015); Buckel et al. (2018)), documenting the development of Glockturmferner from a pure ice glacier to a largely debris covered glacier, presumably transitioning into the ice-cored rock glacier below (Anderson et al., 2018; Jones et al., 2019a; Knight et al., 2019). Along the surface of Hüttekar Rock Glacier, distinct ridges and furrows are visible in the northernmost part). Its gently sloping surface is characterized by distinct furrows and ridges, while the central and southern parts show a smooth and flat surface morphologysteep front rests on top of a slope above Radurschl Valley. Rock glacier debris is composed of orthogneiss derived from the Glockturm massif. Poorly sorted boulders In the southeast, the lower, debris covered parts of Glockturmferner transition into the rock glacier rooting zone. The exact boundary between debris covered glacier and rock glacier is not known. Massive ice is frequently visible beneath a ∼1–2 m thick debris layer in a shallow depression at the southeastern edge of the rock glacier, close to the suspected transition zone. The debris layer consists of poorly sorted boulders with individual blocks measuring up to 4 m, arranged in a loose, clast-supported structureform a heterogeneous surface layer of variable thickness. The blocky surface layer covers a finer-grained , frozen layer dominated by well-graded poorly sorted gravel and sand that is exposed along the rock glacier front. The unfrozen domain of this heterogeneous debris layer increases irregularly in thickness towards the rock glacier front, reaching a maximal thickness of ∼5–10 m.

A small meltwater current from Glockturmferner infiltrates into the rock glacier rooting zone. Water flowing along the permafrost table is visible and audible between boulders at several places in the southern part of the rock glacier, following distinct channels eroded into the ice core. Despite its considerable catchment area, . These water currents follow distinct channels that can be traced below the boulders covering the rock glacier surface. Where visible between the boulders, the channels are up to 1 m wide and 20 cm deep (Supplementary Fig. S1). Surface water bodies in Hüttekar-cirque are restricted to small meltwater lakes and currents in immediate vicinity of the two cirque glaciers. The absence of surface creeks in the lower parts of Hüttekar-cirque indicates that it is drained exclusively by subsurface flow, emerging as a group of small springs at the toe of the slope descending to RadurschltalRadurschl Valley (Fig. 3, Supplementary Fig. S1). The exact number and position of these springs varies during the year, but they are constrained to the sedimentary cone covering the toe of the slope, as evident from 23 field surveys between 2019 and 2022 covering all months. Spring discharge of individual outlets is < 1 l/s and electrical conductivity ranges from 60 to 75 μS/cm, as indicated by repeated measurements during these surveys.

3 Debris flow event

An active, retrogressive debris flow erodes A debris flow eroded the steep slope bordering Hüttekar-cirque to the west (Fig. 2; classification according to Varnes (1978); Cruden and Varnes (1996); Hungr et al. (2014)). Hungr et al. (2014)). The event description given below is based on witness reports by Josef Waldner (staff of the nearby hut Hohenzollernhaus) and Gerhard Schaffenrath (local shepherd). In addition, the debris flow was documented during several field surveys as well as two helicopter flights by Roman Außerlechner, Thomas Figl and Werner Thöny (Geological Survey of Tyrol) on 14 and 26 August 2019, respectively.

Following a moderate precipitation event, destabilization initiated on 13 August 2019, mobilizing a debris volume of several thousand m^3 from the steep rock glacier front (Fig. 4a). The event description is based on in situ observations of Josef Waldner, staff of the nearby hut Hohenzollernhaus (pers. comm.). The debris flow started at 03:00 AM (Central European Summer Time, UTC+2), the main event lasted until about 12:00 PM, followed by reduced debris flow activity that persisted until the next day. Slope failure initiated along an irregularly shaped rupture in ice-cemented debris, exposed at the main scarp (Fig. 4b). Accelerating and disintegrating, the transported mass evolved into a debris flow following a narrow channel down the steep slope below the rock glacier front (Fig. 2, Fig. 3, Supplementary Fig. S2). About 200 m below the initiation zone, the material spread out and formed a deposition fan of 33,000 m^{2}and an estimated volume of 40,000 – 50,000 m^3, thereby damming the river Radurschlbach at an elevation of 2,200 m a. s. l. (Fig. 4c , Fig. 4dand 4d, Supplementary Fig. S1 and S2). Consequently, a lake covering an area of ~60,000 m^2 developed in Radurschl Valley, causing the downstream riverbed to fall dry temporarily (Fig. 4c; Supplementary Fig. S1 and S2). Excavation of a drainage channel lowered the mean water depth from 2 m to 1 m during the following days to prevent a potentially catastrophic outburst. Subsequently, a dam was constructed on the debris fan to restrain future debris flows from damming Radurschlbach again.

Based on in situ observations, aerial photographs, and several surveys conducted before as well as after the debris flow event, a total volume of 40,000 – 50,000 m^3 of mobilized sediment is estimated, providing a rough indication of the event magnitude. The quoted water depths are reconstructed from in situ observations and reviewed by mapping the maximum lake before and after channel excavation, and corresponding volume calculations employing a high-resolution (1 × 1 m) digital terrain model (DTM) based on airborne laserscanning data acquired one year before debris flow occurrence (Government of the Province of Tyrol, 2021a).

Concurrently with During the same night as the debris flow initiation, a thermokarst lake on top of Hüttekar Rock Glacier (~started draining ~350 m behind the initiation zone; debris flow initiation zone and emptied almost completely during the following day, as indicated by local observations (Fig. 3, Fig. 4e, Fig. 4f) drained almost completely within one day, Supplementary Video). The thermokarst lake had started to develop coincidently with the onset of sudden onset of intense snowmelt in early June 2019 within a shallow depression where massive ice within the rock glacier prevented drainage (Fig. 4g). During the last decades, a comparable feature had never been observed before in Hüttekar-cirque, despite frequent visits by hikers, hunters, shepherds, and staff of Hohenzollernhaus. In the stage of its largest extent, the thermokarst lake was approximately 300 m long, up to about 150 m wide and 4–5 m deep, comprising an estimated water volume of $\sim$150,000 m^3.

Effective drainage Effective drainage occurred through a large crevasse (width $\sim$1.5 m, height $\sim$2 m) caused initiation of that formed in association with the debris flow at the front initiation (Fig. 4h). The crevasse was part of a newly formed channel system connecting the thermokarst lake to that part of the rock glacier (Fig. 4e, Fig. 4f, Fig. 4hfront that failed, constituting the debris flow initiation zone. While the exact vertical position of this channel system is not known, clearly discernible and precisely confined collapse structures indicate the trace of this channel network along the rock glacier surface (Supplementary Fig. S1 and S3). Large amounts of water were rapidly transferred to the debris flow initiation zone and torrent beneath. Retrogressive linear erosion visible in the initiation zone where retrogressive linear erosion indicates that concentrated water flow emerged at the main scarp (Fig. 4b), in good agreement with earlier observations of rock glacier front failures (Kummert et al., 2018; Marcer et al., 2020; Kofler et al., 2021). Since then, the depression . During the following months, erosion of loose sediment in the vicinity of the debris flow initiation zone persistently modified its shape and continues to widen it until today. The depression storing the former thermokarst lake never filled again but still shows distinct morphology (Supplementary Fig. S1 and S3).

During the decades preceding the debris flow event, thermokarst lakes had never been observed before on Hüttekar Rock Glacier, despite frequent visits by hikers, hunters, shepherds, and staff of Hohenzollernhaus (Josef Waldner, pers. comm.). In line with these observations, publicly available remote sensing data and historical maps of Hüttekar-cirque do not exhibit any indications of thermokarst lake development on Hüttekar Rock Glacier before June 2019 (evident from Sentinel-2 satellite imagery provided by Copernicus and processed by Sentinel Hub (https://www.sentinel-hub.com/), historical ortho-images and laserscans provided by the Government of the Province of Tyrol, (https://www.data.gv.at/; https://lba.tirol.gv.at/), and historical maps provided by the Government of the Province of Tyrol (https://hik.tirol.gv.at)).

4 Methods

The inherent stability of the slope under consideration determines its response to changes affecting the balance of driving and resisting forces (Glade and Crozier, 2005; Crozier, 2010). Systematic (Crozier, 2010). A systematic identification of factors promoting slope instability is conducted by differentiating (Glade and Crozier, 2005):

(1) predisposing factors (inducing a static setting capable of enhancing that enhances the destabilizing impact of dynamic forcesfactors),

(2) preparatory factors (dynamic forces factors shifting the slope towards a state susceptible to failure), and

(3) triggering factors (dynamic forces factors initiating failure).

Acknowledging that debris flow hazard analysis requires consideration of multiple destabilizing factors , their impact We evaluate the impact of individual factors on slope stability is characterized individually to establish a basis for reconstructing

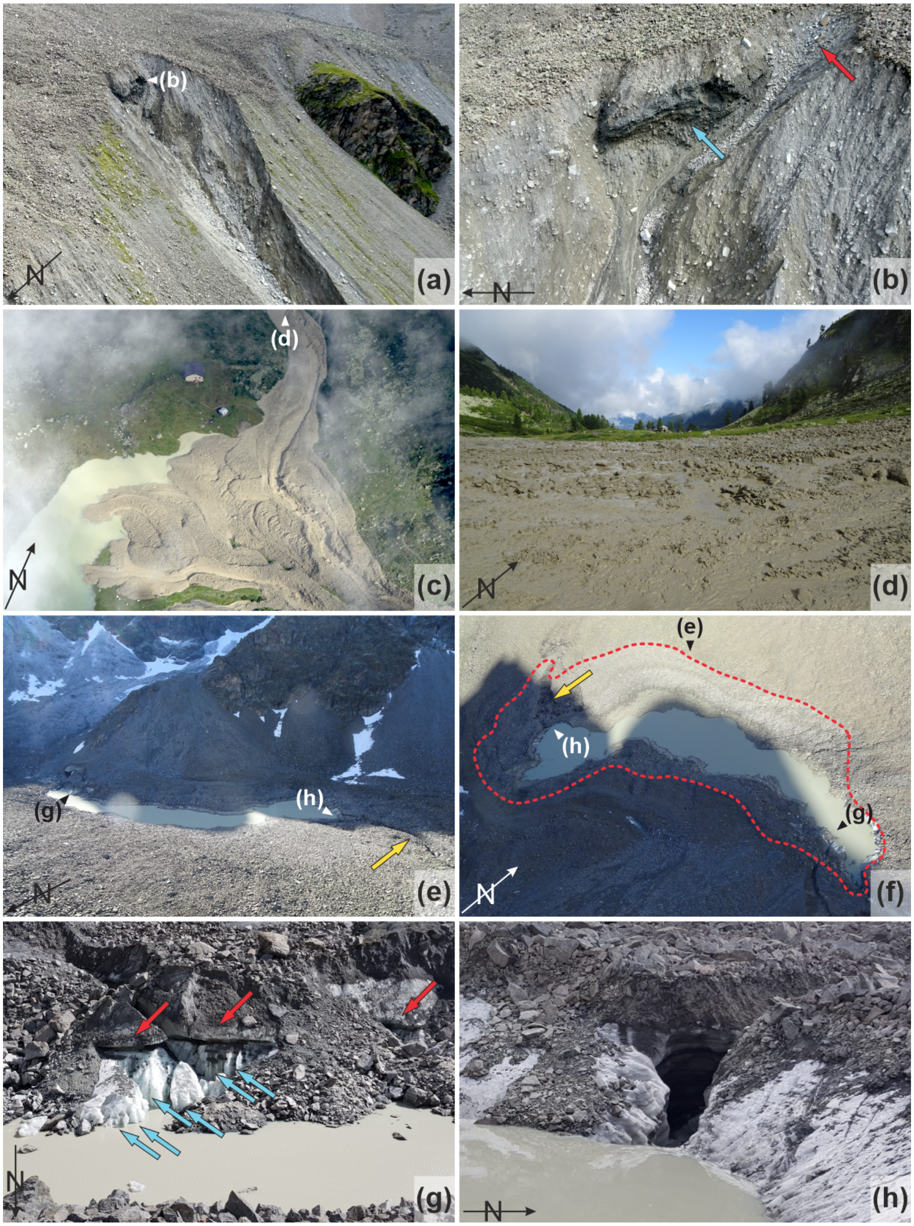

Figure 4. Images documenting the debris flow event that initiated on 13 August 2019. (a) Debris flow initiation zone at the steep front of Hüttekar Rock Glacier. (b) Ice-cemented debris (blue arrow) exposed in the main scarp. Linear retrogressive erosion indicates concentrated water flow (red arrow). (c) Debris flow deposits blocking Radurschlbach. (d) Debris flow material. (e) Thermokarst lake and drainage channel (yellow arrow) on Hüttekar Rock Glacier. (f) Extent of thermokarst lake on 14 August 2019 and maximum extent one day earlier (dashed line). The channel connecting the lake to the debris flow initiation zone is indicated by the yellow arrow. (g) Impermeable ice underlying the thermokarst lake. Blue arrows indicate vertical convexities attributed to thermal convection of water during the lake development. Red arrows indicate undercutting of the ice along the lake shoreline, promoted by thermal convection. (h) Thermokarst channel eroded into the frozen rock glacier core, facilitating rapid drainage of the thermokarst lake. Photographs were taken on 13 August 2019 (g–h) by Josef Waldner, as well as on 14 August 2019 (c–hf) and 26 August 2019 (a–b), respectively, by Roman Außerlechner, Thomas Figl, Werner Thöny, and Josef Waldner.

and identify critical factor combinations to reconstruct the failure mechanism. The chosen methods aim at maximizing comparability to earlier studies on rock glacier front failures and debris flows in periglacial regionsdebris flow initiation at active rock glacier fronts. All analyzed data and employed software are freely available, the respective links are provided in the ’Data availability’ section.

4.1 Predisposing factor analysis

A topographical setting promoting rock glacier destabilization An unfavorable topographical setting is a necessary (but not sufficient) precondition for rock glacier front failure. Attributes significantly affecting slope stability include morphometric parameters such as length, The impact of morphometric factors including slope angle, and curvature (Chowdhury et al., 2010; Reichenbach et al., 2018; Marcer et al., 2019). Sediment erosion, transport, and deposition depend on local energy gradients, available transport vectors, and material properties (Bracken et al., 2015). Collectively, these variables control local loading stresses and the availability of material for subsequent mobilization (Kummert et al., 2018; Kofler et al., 2021). The respective impact of these factors on slope stability length, and curvature is evaluated using a the high-resolution (1 × 1 m) DTM based on airborne laserscanning data acquired two years prior to debris flow occurrence (Government of the Province of Tyrol, 2021a), DTM mentioned above (Government of the Province of Tyrol, 2021a). Morphometric analyses are conducted applying SAGA GIS 2.1.4 for morphometric analyses (Conrad et al., 2015). Slope angle and downslope curvature calculations (Freeman, 1991) are performed using a smoothed (cubic convolution resampling to 10 × 10 m) DTM to detect the fundamental topographical features.

Thermal ground conditions and the presence of subsurface ice affect the shear strength of involved materials, alter groundwater flow patterns, and impact the storage and release of water by thermokarst evolution. The spatial permafrost distribution is estimated by taking recourse to the Alpine Permafrost Index Map, providing a static proxy for potential permafrost occurrence and its spatial coherence (Boeckli et al., 2012b, a). While the dynamic effect of climate change is not considered explicitly by the index map, permafrost degradation is expected to intensify close to the lower permafrost boundary (Marcer et al., 2019). The local influence of topography on the energy available for permafrost degradation (Scherler et al., 2014; Marcer et al., 2019) is assessed by calculating the potential incoming solar radiation based on the DTM(Hock, 2005; Cuffey and Paterson, 2010). Calculations of mean annual solar radiation under clear-sky conditions are performed employing GRASS GIS 8.0 (GRASS Development Team, 2022) module r.sun (Hofierka et al., 2007), assuming an average surface albedo of 0.2.

The mechanics of debris flows are largely determined by solid-fluid interactions, rendering grain size distribution and water content major variables driving flow behavior (Iverson, 1997). The rate of water supply is determined by the permeability of sediments above the initiation zone. Geotechnical and hydrogeological characteristics of the materials involved are inspected by analyzing the grain size distribution of the rock glacier surface layer at one coarse-grained and three relatively fine-grained domains (sampling locations of the rock glacier front material is inspected by wet sieving of four samples taken in 2009, 50 m southwest of the later debris flow initiation zone (position indicated in Fig. 3). At each location the maximum diameter of 200 clasts lying side by side is measured in an area of approximately 2 × 2 m (fine grained domains) to 5 × 5 m (coarse grained domain). The grain size distribution of the poorly sorted sediment layer below the blocky surface is analyzed by manual wet sieving of a sample taken at the steep rock glacierfront.

The geometry of the Due to the heterogeneous structure of the rock glacier, these samples are not representative for the grain size composition of the entire rock glacier. However, considering the proximity of the sampling locations to the subsequent debris flow initiation zone, and the dangerous sampling conditions at active rock glacier front depends on the dynamic balance between rock glacier kinematics and erosion rates (Kummert and Delaloye, 2018). fronts in general, we consider these samples reasonable approximations to the grain size composition of the debris flow source material.

4.2 Preparatory factor analysis

Time series of ortho-images are used to quantify rock glacier surface displacement rates and the evolution of surface features indicating destabilization (including cracks, crevasses, and scarps; Avian et al. (2007); Roer et al. (2008); Delaloye et al. (2013); Marcer et al. (2019);). The analyzed ortho-images provided by the Government of the Province of Tyrol (2021b))exhibit a spatial resolution of 20 cm and are provided as Supplementary Fig. S3 (Government of the Province of Tyrol, 2021b). In the observation period 1970–2020, 200 prominent blocks, geometrically well distributed on the rock glacier surface, are visually identified at each every ortho-image epoch to approximate the horizontal surface displacement rate rates at the respective location within single periods (1970-2003-2007-2010-2020, Avian et al. (2009); Kummert and Delaloye (2018)). Additionally, the position of the rock glacier front line (top of the erosional slope) is mapped at every epoch. Both analyses provide the basis for assessing the kinetic patterns on the rock glacier surface (Avian et al., 2009; Kummert and Delaloye, 2018). Visual detectability within optical imagery is approximately half of a pixel size (in this case 10 cm). Assessed surface displacement rates cover at least 3 years, thus minimum rates of 3–4 cm are detectable.

Climatic factors and their progressive change exert a key control on slope stability (Gariano and Guzzetti, 2016; Patton et al., 2019). Alterations in volume and intensity of rainfall, snowmelt and ice melt affect subsurface water content, pore-water pressure and seepage forces (Ikeda et al., 2008; Cicoira et al., 2019; Patton et al., 2019)The hydrometeorological conditions preceding the debris flow are contextualized by comparing them to past conditions. The long-term evolution of air temperature and precipitation in Hüttekar-cirque is evaluated using the gridded (1 × 1 km) SPARTACUS data set (Spatiotemporal Reanalysis Dataset for Climate in Austria; Hiebl and Frei (2016, 2018)). The dataset is continuously updated by GeoSphere Austria. Daily precipitation totals and 24 hour mean air temperature data observed from 1976 to 2019 are extracted and averaged across Hüttekar-cirque. Specific aspects of the local climate are explored by calculating The averaging domain corresponds to the Hüttekar Rock Glacier catchment as specified by Wagner et al. (2020). We calculate the annual positive degree day sum (daily mean air temperature > 0 °C) as a proxy for available melting energy, as well as and the precipitation due to very wet days (> 95th percentile) reflecting which reflects the annual magnitude of heavy precipitation events (Klein Tank et al., 2009; Cuffey and Paterson, 2010). Considering that the hydrometeorological conditions preceding the debris flow determine the critical amount of water necessary to initiate failure (Crozier, 2010), the The impact of these climate indices is assessed by comparing their respective values during summer 2019 (01 June–13 August (failure date)) to previous years (1976–2019). To estimate changes in their central tendency, trend direction and rate of change are evaluated using the nonparametric seasonal Mann Kendall test (Theil, 1950; Sen, 1968; Hirsch et al., 1982; Hirsch and Slack, 1984)and Theil-Sen slope, respectively (Hirsch et al., 1982; Hirsch and Slack, 1984). Calculations are performed employing R packages 'rkt' 1.6 (Marchetto, 2021) and 'climdex.pcic' 1.1 (Bronaugh, 2020), implemented in R 4.2.0 (R Core Team, 2022).

In the Alps, individual storms exhibit strong intensity gradients at length scales < 5 km (i. e. below the basic length-to-crest scale; Haiden et al. (2011); Nikolopoulos et al. (2014, 2015a); Marra et al. (2016); Destro et al. (2017)). The combination of weather station data and remote sensing information allows the detection of individual event characteristics (Haiden et al., 2011; Borga et al., 2014; Marra et al., 2014, 2016; Destro et al., 2017). Detailed ($\sim$hourly) temporal resolution of precipitation data is necessary to avoid biased estimates of rainfall intensity and duration (Marra, 2019). Meteorological analyses at time intervals from hours to months are thus based on the INCA system (Integrated Nowcasting through Comprehensive Analysis; Haiden et al. (2011)), providing gridded (1 × 1 km) data sets at hourly temporal resolution. Inclusion of 12 weather stations at a distance < 25 km from Hüttekar-cirque, in combination with C-band radar measurements and Meteosat Second Generation Satellite Products, allows assessing the spatial and temporal patterns of meteorological conditions at the study site.

For each winter season, the cumulated snowmelt volume in Hüttekar-cirque is calculated and compared to the 2018/19 season. The rate of snowmelt is approximated by the respective seasonal average during the time span between maximal snow volume and complete ablation of the winter snow cover, in analogy to Kofler et al. (2021). Snow cover development is assessed using the spatially distributed, physically based snow cover model SNOWGRID (Olefs et al., 2013). It The model employs a simple two-layer scheme, considering settling, the heat and liquid water content of the snow cover, snowline depression effects and the energy added by rain. For every time step and layer, the state variables snow Snow density, snow water equivalent, snow temperature, liquid water content, bottom liquid water flux, and surface albedo are calculated . The primary focus of the model is to obtain a high-resolution representation of their spatial distribution and to provide fast calculations on a large gridat hourly resolution. The model employs a 100 × 100 m bilinear interpolation of the INCA data set (Integrated Nowcasting through Comprehensive Analysis; Haiden et al. (2011)) in combination with schemes for radiation and cloudiness developed at the Central Institute for Meteorology and Geodynamics (Austria). These are based on ground measurements, satellite products, and high quality solar and terrestrial radiation data (Olefs et al., 2013, 2016). For each winter season, the cumulated snowmelt volume in Hüttekar-cirque is calculated and compared to the 2018/19 season. The rate of snowmelt is approximated by the respective seasonal average during the time span between maximal snow volume and complete ablation of the winter snow cover (Kofler et al., 2021). The resulting snow cover data are routinely evaluated and validated by GeoSphere Austria using more than 50 station measurements of snow depth, additional measurements regarding snow depth and snow water equivalent (5 stations along with more than 200 individual measurements), snow depth measurements employing laser sensors, winter mass balance measurements of glaciers within the model domain, spatial validation of snow cover extent using satellite-based fractional snow cover area provided by MODIS, as well as cumulative runoff data (Olefs et al., 2020).

Glacial meltwater infiltrates directly from Glockturmferner and indirectly from Hüttekarferner into the rock glacier (Fig. 3), thus the The total volume and average rate of ice melt is are calculated for each year between ablation of the snow cover and 13 August (failure date), based on the surface energy balance for the respective glacier (Hock, 2005; Cuffey and Paterson, 2010). Ice melt rates are calculated at hourly intervals by evaluating radiative, turbulent, and advective energy fluxes per glacier derived from INCA, assuming a constant glacier surface temperature of 0 °C (considered a reasonable approximation for the ablation zones of temperate glaciers during the summer season; Cuffey and Paterson (2010)). Shortwave net radiation is calculated by evaluating global radiation, accounting for the reflective and shadowing influences of topography as outlined in Sect. 4.1. Atmospheric conditions influencing longwave radiation are considered following Greuell et al. (1997) and Oerlemans (2000). Sensible and latent heat fluxes are calculated by parameterization of the respective transport processes based on turbulence similarity (Cuffey and Paterson, 2010). The rainfall heat flux is estimated assuming that rainfall temperature approaches the near-surface air temperature. Physical specifications and plausibility evaluation are provided in Appendix A.

4.3 Triggering factor analysis

Rainfall-induced debris flows are triggered by infiltration rates exceeding subsurface drainage rates and the corresponding alteration of pore-water pressures (Sidle, 1984; Johnson and Sitar, 1990; Anderson and Sitar, 1995; Wieczorek, 1996; Wieczorek and Glade, 2005; Crozier, 2010). Infiltrating water adversely affects slope stability by adding additional weight while simultaneously decreasing shear strength, either by lowering effective stresses in response to increasing positive pore-water pressures or by eliminating suction due to declining negative pore-water pressures (Johnson and Sitar, 1990; Anderson and Sitar, 1995; Chowdhury et al., 2010; Crozier, 2010). In order to evaluate the impact of the storm rainfall event immediately preceding the debris flow on 13 August 2019, rainfall time series are extracted from INCA at hourly resolution, averaged across the potentially contributing area (Hüttekar-cirque), and discretized into single events by defining a minimum of 24 hours between individual events (Nikolopoulos et al., 2015b; Marra et al., 2016). Inclusion of 12 weather stations at a distance < 25 km from Hüttekar-cirque, in combination with C-band radar measurements and Meteosat Second Generation Satellite Products, allows reliable identification of event characteristics at the study site. Calculations are performed employing the R package 'IETD' 1.0 (Duque, 2020), implemented in R 4.2.0 (R Core Team, 2022). The resulting ensemble of rainfall event duration, volume, and average intensity is analyzed by conducting a frequency analysis. The severity of individual events is assessed employing the frequentist approach developed by Brunetti et al. (2010) and Peruccacci et al. (2012). The rainfall event characteristics immediately preceding the slope failure are compared to earlier events hitting Hüttekar-cirque as well as to regional critical rainfall thresholds for debris flow initiation (Nikolopoulos et al., 2015b; Marra et al., 2016).

Glacial lake outbursts evolving into debris flows are commonly initiated by mechanical failure of the dam or by rapid expansion of the lake drainage system through thermal erosion of ground ice. The volume and geometry of the impounded reservoir, dam characteristics, failure mechanism, downstream topography and sediment availability control the hazard potential (Clague and Evans, 1994). The development of thermokarst features, including meltwater lakes and channels , is highly sensitive to thermal ground conditions and their response to climate change (Kääb and Haeberli, 2001). The spatiotemporal evolution of the thermokarst lake on Hüttekar Rock Glacier is deduced by combining Sentinel-2 multi-spectral satellite data and the latest (2017/18) available DTM, characterizing the lake surface area dynamics and corresponding water volume development (modified Copernicus data 2020 processed by Sentinel Hub; Sentinel Hub (2020); Government of the Province of Tyrol (2021a)). Due to the dynamic nature of Breakthrough of thermokarst channels within the rock glacier surface, volume estimates are considered rough estimates, failing to account for water stored in the pore space and potential intra-permafrost channels. Breakthrough of thermokarst channels is facilitated by a positive feedback mechanism of energy transfer along the channel system inducing ice melt and channel enlargement, which in turn increases discharge and accelerates channel growth (Nye, 1976; Clarke, 1982, 2003; Spring and Hutter, 1981a, b; Clague and Evans, 1994; Walder and Costa, 1996; Huggel et al., 2004; Cuffey and Paterson, 2010; Clague and O'Connor, 2015)(Huggel et al., 2004; Clague and O'Connor, 2015). Dimensional analysis indicates that the energy provided by the upstream water body governs expansion rates of the drainage system (Clarke, 1982, 2003; Cuffey and Paterson, 2010). The prediction of the specific channel system evolution is impossible without exact knowledge of its geometry and hydraulic properties. However, the estimation of the meltwater thermokarst lake energy budget provides represents a measure of the total energy available for thermokarst development. Undercutting and vertical pipe structures eroded into the ice along the lake shoreline provide field evidence for thermal convection (Fig. 4g), promoting energy turnover and melting of ice beneath the lake while constraining the surface water temperature to < 4 °C due to negative thermal expansion (Haeberli et al., 2001; Kääb and Haeberli, 2001; Werder et al., 2010). Rapid transfer of energy exchanged at the lake surface to the ice sealing the lake bottom keeps the water at roughly constant temperature, thus allowing for an assessment of the lake energy balance based on INCA data (physical specifications are provided in Appendix A). The spatiotemporal evolution of the thermokarst lake on Hüttekar Rock Glacier is deduced by combining Sentinel-2 multi-spectral satellite data and the latest (2018) available DTM, characterizing the lake surface area dynamics and corresponding water volume development (modified Copernicus data 2020 processed by Sentinel Hub (2020); Government of the Province of Tyrol (2021a)). Due to the dynamic nature of the rock glacier surface, volume estimates are considered rough estimates, failing to account for water stored in the pore space and potential intra-permafrost channels.

5 Results

A systematic evaluation of destabilizing factors and adverse combinations thereof requires an individual evaluation of every potentially contributing factor.

5.1 Predisposing factors

Morphometric analysis of the study area reveals several features promoting debris flow development. The slope (900 m long and 400 m in elevation difference) bordering Hüttekar-cirque to the west shows a very steep, convex top and a steep, concave

Table 2. Morphometric analysis based on a high-resolution DTM acquired in the period 2017/2018 one year before debris flow occurrence by the Government of the Province of Tyrol (2021a). Results are given as averages across the debris flow initiation zone, transportation zone, and zone of deposition, respectively (indicated in Fig. 3)

Morphometric parameter	Initiation zone	Transportation zone	Zone of deposition
Mean altitude (m a.s.l.)	2,541	2,362	2,227
Mean slope gradient (°)	33.0	25.0	14.2
Mean downslope curvature (-)	+0.05	-0.08	-0.08

main part (Fig. 5a, Fig. 5b). Prior to landslide initiation, the prospective initiation zone was characterized by steep slope angle and convex downslope curvature (Table 2). The channel below the It formed a part of the 400 m wide and 100 m high rock glacier frontwas less steep and concave, while the debris fan was already comparatively flat before the 2019 debris flow (Table 2). Irregular micromorphology, depositional levees, and boulder trains document earlier debris flows (Fig. 2, Fig. 5; Soeters and van Westen (1996); Pack (2005); Hungr et al. (2014)). Material eroded at the , bounded to the top by a distinct erosional edge separating it from the flat rock glacier surface. The steep rock glacier front is available for subsequent mobilization further downslope, inhibiting the formation of a stabilizing debris accumulation at the toe of the rock glacier front (Kummert and Delaloye, 2018; Kummert et al., 2018; Kofler et al., 2021)(35° on average) exhibited roughly homogeneous appearance, except for two bedrock outcrops in its southern part. A direct comparison of this area before and after the debris flow event is provided in Supplementary Fig. S4.

Assessment of thermal ground conditions indicates that the debris flow initiation site is subjected to a high energy environment. Potential incoming solar radiation reaches 2,135 kWh m^{-2} a^{-1} (Fig. 5c). The Alpine Permafrost Index Map indicates that the initiation zone is located at the lower permafrost boundary, with permafrost preserved only in very favorable conditions (Fig. 5d). Collectively, the convex morphology and exposed position, strong potential radiation and unfavorable permafrost index are conducive to an advanced stage of permafrost degradation, increased water contents, and large amounts of unfrozen, loose sediment susceptible to mobilization (Marcer et al., 2019).

Grain size analyses indicate that the blocky surface layer of Hüttekar Rock Glacier is composed of poorly sorted, coarse-grained sediment. The finer-grained parts, measured on three locations (1–3; positions given in Fig. 3), show an average grain size of 11.6, 12.8, and 16.0 cm, respectively. The coarse-grained site (4) exhibits an average grain size of 65.6 cm, documenting the heterogeneous structure of the blocky surface layer. Figure 6a displays the respective grain-size distributions. Due to the subordinate presence of components smaller than gravel (largely matrix-free surface layer), the rock glacier classifies as bouldery rock glacier sensu Ikeda and Matsuoka (2006). These characteristics indicate a permeable surface layer exhibiting high infiltration capacity and low hydraulic resistance to water flowing along the permafrost table.Sieve analyses of samples 5–8 taken at the rock glacier front material (Fig. 6b, positions indicated in Fig. 36) show that gravel (64 %) and sand (25 %) are

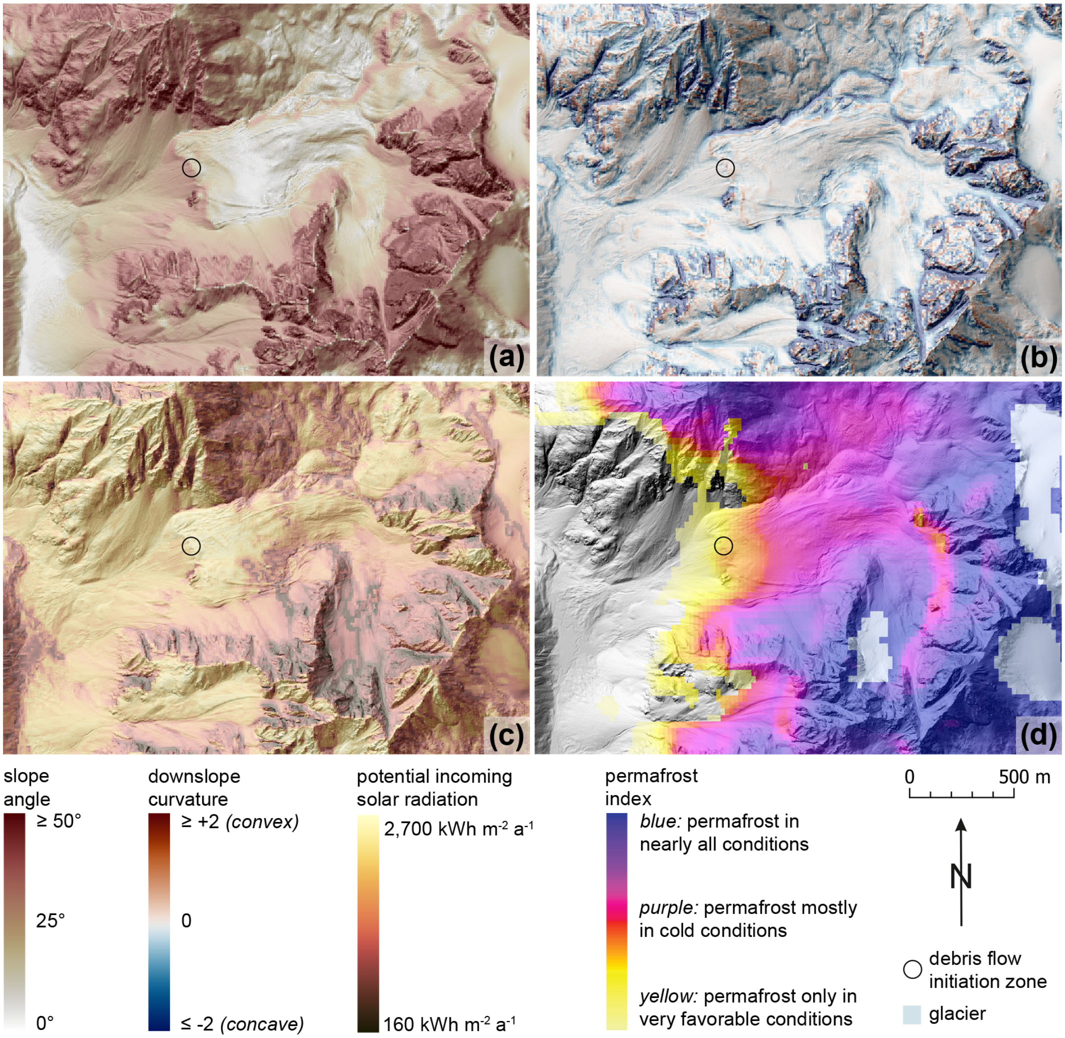

Figure 5. Spatial distribution of predisposing factors across Hüttekar-cirque prior to debris flow initiation. (a) Slope angle, indicating that the debris flow initiated in steep terrain (33°). (b) Downslope curvature, demonstrating that convex topography prevailed in the initiation zone before the debris flow event (+0.05). (c) Potential incoming solar radiation, illustrating the high-energy environment characterizing the debris flow initiation zone (2135 kWh m^{-2} a^{-1}). (d) Permafrost index, indicating that the debris flow initiated close to the lower permafrost boundary (Boeckli et al., 2012a). Terrain analyses are based on a high-resolution DTM acquired in the period 2017/2018 one year before debris flow occurrence by the Government of the Province of Tyrol (2021a). Perceptually uniform and color-vision-deficiency color-vision deficiency friendly color maps ramps are provided by Crameri (2018).

the dominating grain sizes, while the amount of clay and silt is very low (< 1 %). Detailed results are provided in Supplementary Table S1. The samples are extremely poorly sorted (4.4 after Folk and Ward (1957)). Loose deposits of sediments exhibiting similar grain size distributions are well known to respond to shearing in a contractive manner and constitute characteristic debris

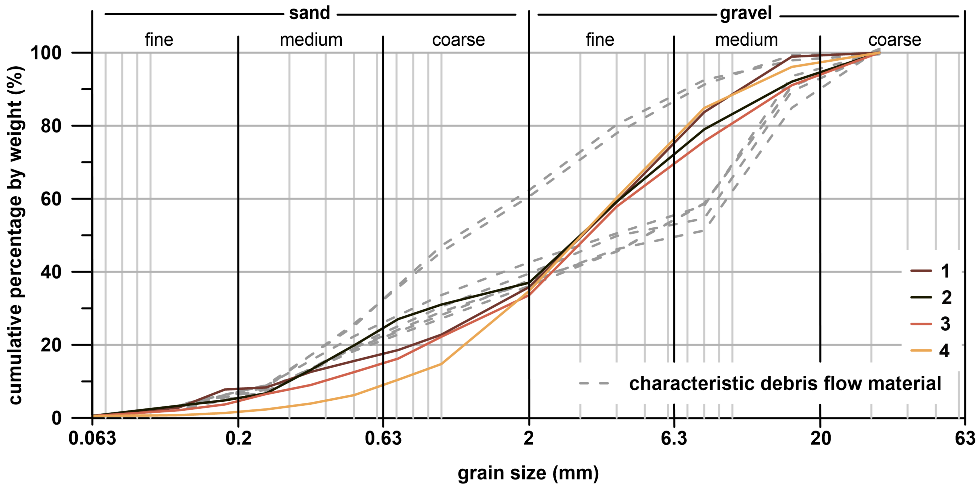

Figure 6. Grain-size distributions of material composing the rock glacier front. The corresponding sampling locations are 50 m southwest of the debris flow initiation zone, as indicated in Fig. 3. Dashed grey lines represent source compositions of a set of experimentally investigated debris flows showing contractive shear response and undrained failure (USGS debris flow flume; Major (1996); Iverson (1997); Iverson et al. (1997)). Classification according to ISO 14688-1 (International Organization for Standardization, 2017).

flow material (Iverson, 1997; Savage and Baum, 2005). Experimental investigations of similarly composed source material confirm these observations(dashed lines in Fig. 6b), identifying contractive response to shearing and pore pressure diffusion timescales exceeding the duration of debris flow motion as major prerequisites for mobilization (Major, 1996; Iverson, 1997). Provided sufficient water is available to keep (dashed lines in Fig. 6; Major (1996); Iverson (1997)).

The 80 m wide and 200 m long debris flow initiation zone eroded into the rock glacier debris saturated, these characteristics promote the development of undrained loading conditions, high sensitivity of effective stresses to sediment compaction and perpetually high excess pore-water pressures in response to deformation (Major, 1996; Iverson, 1997; Major et al., 1997). These features document the compositional propensity of front exposes its internal structure. The irregular, concave niche exhibits steep flanks that are up to 30 m high and composed of loose, poorly-sorted sediment (Fig. 4a and 4b; Supplementary Fig. S1–S4). Its top represents the terminus of a collapse structure network connecting it to the former position of the thermokarst lake (Supplementary Fig. S1, S3, and S4), with linear erosion features indicating concentrated emergence of water. After the debris flow initiation, frozen material was exposed immediately below the top (Fig. 4a and 4b; Supplementary Fig. S2). Assessment of thermal ground conditions indicates that the debris flow initiation zone is subjected to a high energy environment. Potential incoming solar radiation reaches 2,135 kWh m^{-2} a^{-1} (Fig. 5c). The Alpine Permafrost Index Map indicates that the initiation zone is located at the lower permafrost boundary, with permafrost preserved only in very favorable conditions (Fig. 5d).

The channel below the rock glacier front to debris flow mobilizationis less steep and concave (Table 2). The debris fan was already comparatively flat before the 2019 debris flow (Table 2). Irregular micromorphology, depositional levees, and boulder trains document earlier debris flows (Fig. 2, Fig. 5; Supplementary Fig. S2; Soeters and van Westen (1996); Pack (2005); Hungr et al. (2014)).

Collectively, the convex morphology and exposed position, strong potential radiation and unfavorable permafrost index are conducive to an advanced stage of permafrost degradation, increased water contents, and large amounts of unfrozen, loose sediment susceptible to mobilization (Marcer et al., 2019).

5.2 Preparatory factors

Analysis of multi-temporal ortho-images indicates roughly constant, moderate surface displacement rates (Supplementary Fig. S5). The kinematics of the rock glacier surface show mean annual surface displacement rates of the 200 prominent blocks ranging from 1–50 cm a^{-1} (mean: 14 15 cm a^{-1}) in the observation period of 1970–2020. Data for individual blocks and summary statistics are provided in Supplementary Table S2. The position of the rock glacier front fluctuates non-directionally (amplitude 3–7 m), indicating that steady erosion of the front approximately balances rock glacier movement, thus ensuring an invariant long-term front geometry (Kummert and Delaloye, 2018). While destabilization of rock glaciers is frequently characterized by accelerating surface deformation rates and the development . The absence of surface discontinuities such as cracks and crevasses, the absence of these features on Hüttekar Rock Glacier does not point towards and the constant surface displacement rates do not indicate general destabilization of the rock glacier before the 2019 debris flow. However, after the debris flow, a cluster of collapse structures connecting the shallow depression hosting that hosted the thermokarst lake and the debris flow initiation zone is clearly recognizable (Fig. S2; Government of the Province of Tyrol (2021b)Supplementary Fig. S3).

Analyzing the long-term (1976–2019) climate signal highlights the distinct hydrometeorological characteristics of the The months preceding the failure and the respective debris flow were characterized by warm and dry conditions, on top of an exceptionally strong long-term trends trend of increasing air temperature in Hüttekar-cirque (Table 3). In 2019, the summer months show exceptionally high air temperatures compared to the long-term average (+2.4 °C). The high positive degree day sum (+161 °C) reflects the large amount of energy available for melting (Table 3). Total precipitation is moderately low (-17 mm) and slightly concentrated on very wet days (+5 mm) with respect to the long-term average (Table 3). The climate data record record shows significantly increasing air temperature (+0.05 °C a^{-1}, exceeding corresponding trends at the global and European Alps scale (+0.02(±0.01) °C a^{-1} and +0.03(±0.02) °C a^{-1}, respectively; Hock et al. (2019))) and positive degree day sum (+7.2 °C a^{-1}). In contrast, neither total precipitation nor precipitation due to very wet days increase increases significantly during the 43 years preceding the debris flow (at the $\alpha = 0.05$ level). Recapitulating, the months preceding the debris flow are characterized by warm and dry conditions, on top of an exceptionally strong long-term trend of increasing air temperature in Hüttekar-cirque.

Figure 7 depicts the inter-annual comparison of snowmelt, ice melt and rainfall (normalized to catchment area), indicating moderately wet conditions anteceding the debris flow. Intense snowmelt and ice melt (11.2 and 2.7 mm d^{-1}, respectively) reflect the high energy available in 2019, in agreement with the high positive degree day sum reported above. The winter

Table 3. Climate analysis highlighting the warm and moderately dry conditions prevailing during summer 2019, preceding the debris flow. In addition, air temperature and positive degree day sum show a strong long-term trend, promoting permafrost degradation in Hüttekar-cirque. Angle brackets indicate average values, insignificant trends (at the $\alpha = 0.05$ level) are given in rounded brackets.

Parameter	**Air temperature**	**Positive degree day sum**	**Precipitation**	**Precipitation due to very wet days**
Summer 2019	7.0 °C	519 °C	329 mm	102 mm
Summer <1976–2019>	4.6 °C	358 °C	346 mm	97 mm
<2019>	-1.5 °C	842 °C	1,348 mm	359 mm
<1976–2019>	-2.5 °C	653 °C	1,042 mm	245 mm
Trend magnitude	+0.05 °C a^{-1}	+7.2 °C a^{-1}	(+0.13 mm a^{-1})	(+0.05 mm a^{-1})
Trend significance (*p*-value)	2.4×10^{-13}	3.3×10^{-7}	(3.7×10^{-1})	(9.9×10^{-1})

season preceding the debris flow is was characterized by a prominent snow cover, almost monotonically gaining volume until 29 May 2019, roughly restricting meltwater production to June . The long-lasting snow cover and rapid snowmelt (2019. The late onset of snowmelt is responsible for the unusually high peak, followed by high solar exposure and extraordinarily warm air temperatures driving rapid ablation in June. The high rates of meltwater production caused widespread flooding in Tyrol, despite the fact that June 2019 was a particularly dry month (Hydrological Service of Tyrol, 2019; Hübl and Beck, 2020). Intense snowmelt and ice melt rates in Hüttekar-cirque reflect the strong atmospheric energy input in 2019 (11.2 and 2.7 mm d^{-1}, respectively; Fig. 7b)is in excellent agreement with observations throughout Tyrol (Hydrological Service of Tyrol, 2019). Comparing total volumes .

In contrast to the high intensity of the melting processes, comparing total volumes of snowmelt, ice melt and rainfall indicates inconspicuous overall conditions in 2019 (Fig. 7c). As a first-order approximation, we compare cumulative volumes between 1 January 2019 and 13 August 2019 (failure date) to earlier years (consistently totalized from 1 January to 13 August), acknowledging that the relatively short record precludes statistically substantiated conclusions. Compared to the four years before 2019 (for which continuous SNOWGRID data are available), the total snow melt volume exceeds the 5-year-average by 19 %, while both the total ice melt volume and rainfall volume are slightly below this average (-3 % and -2 %, respectively). The rapid snowmelt efficiently eliminated the snow cover in Hüttekar-cirque, so that snowmelt ceased on 22 July 2019, i.e. 22 days before the debris flow initiated.

The combination of large amounts of snow available for melting and abnormally warm and dry weather conditions resulted in rapid and extensive meltwater production, thus favoring the ponding of meltwater on the surface of Hüttekar Rock Glacier. The continuously high atmospheric energy input promoted the subsequent development of the thermokarst lake from 3 June 2019 to 13 August 2019 described in Sect. 5.3. Summarizing, major hydrometeorological factors distinguishing 2019 from earlier years are the rapid and late snowmelt, the high energy environment during the summer months, and the storage of water in the newly formed thermokarst lake.

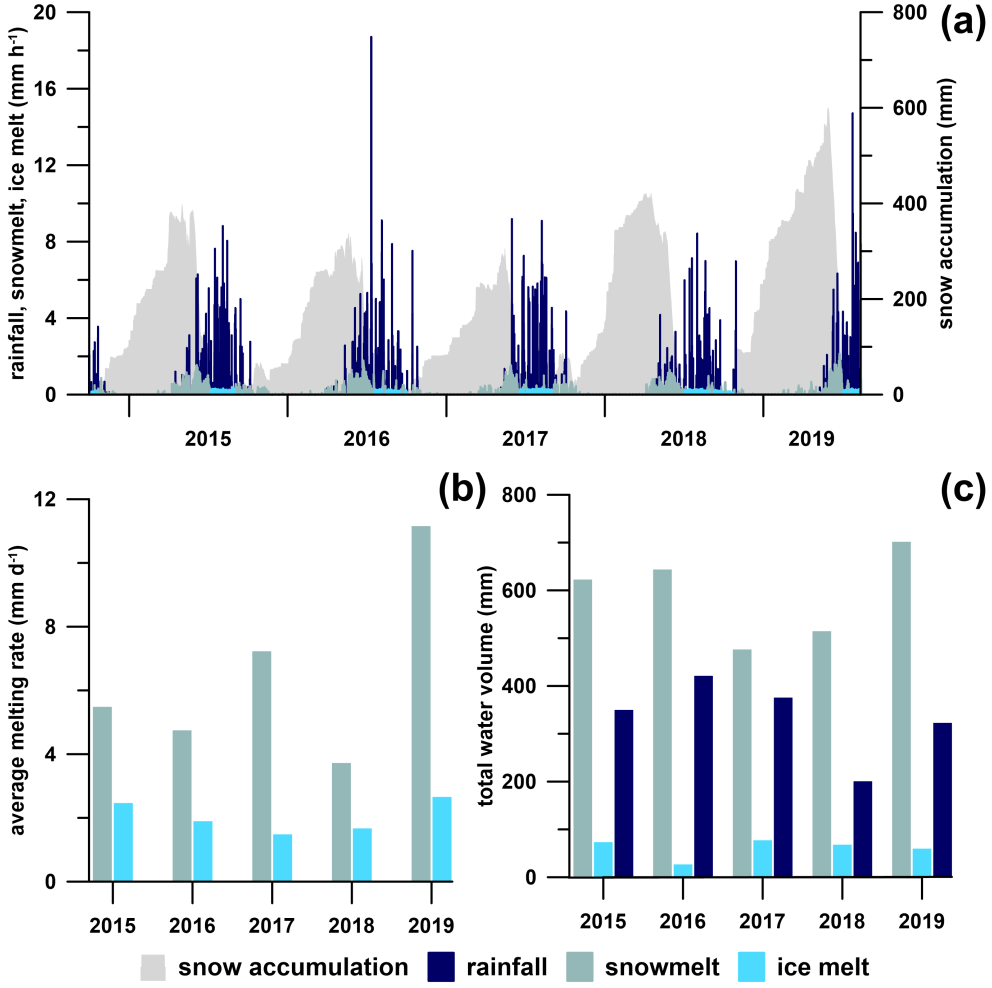

Figure 7. (a) Time series of rainfall, snowmelt and ice melt in Hüttekar based on INCA (Haiden et al., 2011) and SNOWGRID (Olefs et al., 2013). The snow cover dynamics in spring 2019 differ from the preceding years by the late and rapid snowmelt. (b) Average snowmelt and ice melt rates for individual years. Spring 2019 is characterized by exceptionally high snowmelt rates. (c) Total water volumes (between 01 January and 13 August) per year, attributed to rainfall, snowmelt and ice melt, respectively. Despite the different snow cover dynamics in spring 2019, the total meltwater volume exceeds the respective volume of the preceding years only slightly.

5.3 Triggering factors

The rainfall event preceding the debris flow lasted for 74 h at an average intensity of 0.54 mm h^{-1} (total rainfall volume ∼40 mm). The frequency analysis shows that 12 % of earlier rainfall events hitting Hüttekar-cirque exceeded it in severity (Fig. 8). The event does not exceed did not cross the regional critical rainfall thresholds for debris flow initiation during the summer season with respect to intensity-duration (Fig. 8a; Nikolopoulos et al. (2015b)) and volume-duration (Fig. 8b; Marra

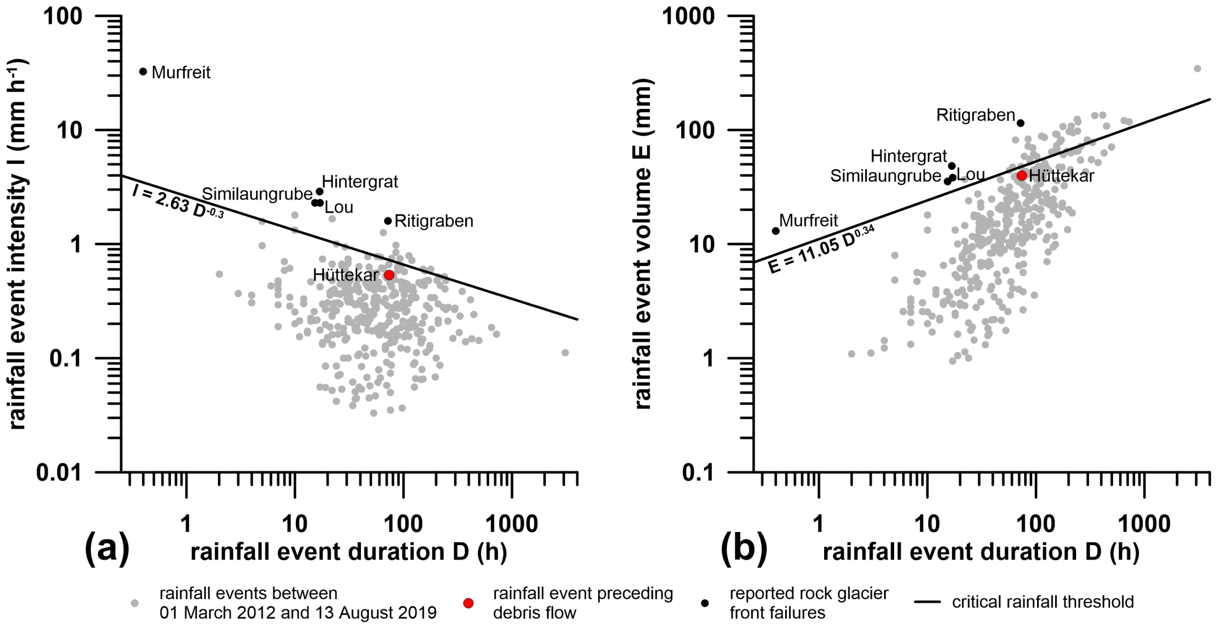

Figure 8. Rainfall event frequency analysis with respect to (a) rainfall intensity-duration intensity I vs. rainfall event duration D and (b) rainfall volume-duration based on INCA (Haiden et al., 2011)event volume E vs. The rainfall event preceding the Hüttekar debris flow (red dot) was neither especially intense nor especially persistent with respect to earlier rainfall events hitting Hüttekar-cirque (grey dots), critical rainfall thresholds (black lines) and rainfall events triggering documented rock glacier front failures in the European Alps (black dots) duration D based on INCA (note logarithmic scale). Regional thresholds describing minimum conditions for rainfall-induced debris flows are based on Nikolopoulos et al. (2015b) and Marra et al. (2016), with equations given below the corresponding lines (thresholds are representative for the summer season). Characteristics of documented triggering rainfall events are based on Lugon and Stoffel (2010); Krainer et al. (2012); Kofler et al. (2021); Marcer et al. (2020).

et al. (2016)), although these are regarded conservative estimates (Wieczorek and Guzzetti, 2000; Guzzetti et al., 2007). These characteristics distinctly contrast with the rainfall events preceding well documented rock glacier front failures debris flows from other rock glacier fronts in the European Alpsthat occurred . Those occurred most often in response to heavy rainfall (Fig. 8): the Ritigraben event on 24 September 1993 (Lugon and Stoffel, 2010), the Murfreit event on 02 July 2003 (Krainer et al., 2012), the Hintergrat and Similaungrube events, both on 13 August 2014 (Kofler et al., 2021), as well as the Lou event on 14 August 2015 (Marcer et al., 2020). In contrast, the rainfall event preceding the debris flow at Hüttekar Rock Glacier was neither especially intense, nor especially persistent.

Field observations as well as satellite data analysis detect the rapid evolution and drainage of the thermokarst lake that was formed on the rock glacier surface before the debris flow. Sentinel-2 satellite imagery indicates water pooling in the depression on 03 June 2019, when snow still covered large parts of the rock glacier catchment (520 mm average snow water equivalent based on SNOWGRID). The thermokarst lake evolved over a period of 10 weeks, but drained within hours through a newly

Table 4. Thermokarst lake development based on INCA (Haiden et al., 2011), Sentinel-2 satellite data (Sentinel Hub, 2020) and the most recent (20172018) high-resolution DTM of the rock glacier surface (Government of the Province of Tyrol, 2021a).

Date	Surface area (m^2)	Water volume (m^3)[a]	Mean water depth (m)	Total energy input (J)[b]	Total ice melt (m^3)[b]
01 June 2019	0	0	0	0	0
03 June 2019	1,520	1,320	0.9	2.9×10^{10}	100
13 June 2019	21,370	68,340	3.2	1.6×10^{12}	5,410
16 June 2019	26,380	97,020	3.7	2.7×10^{12}	8,850
18 June 2019	28,570	110,760	3.9	3.4×10^{12}	11,180
26 June 2019	31,670	131,870	4.2	6.3×10^{12}	20,940
28 June 2019	34,010	148,290	4.4	7.3×10^{12}	24,220
01 July 2019	35,650	158,770	4.5	8.8×10^{12}	29,380
06 July 2019	36,400	162,370	4.5	1.1×10^{13}	36,280
16 July 2019	36,960	166,040	4.5	1.4×10^{13}	47,050
23 July 2019	36,960	166,040	4.5	1.7×10^{13}	57,550
26 July 2019	36,960	166,040	4.5	1.9×10^{13}	63,090
13 August 2019	36,960	166,040	4.5	2.6×10^{13}	87,480

[a] estimate based on DTM (2018) [b] since 01 June 2019

formed channel, indicating that the characteristic time scale of thermokarst breakthrough is shorter than the summer season (Fig. 4e-h, Fig. S2). Comparing snow cover and lake development shows that the latter lake gained most of its volume during the intense snowmelt period in June (Fig. 8a7a). Linear interpolation of the lake surface area between the cloud-free satellite imagery dates enables the calculation of the total energy input to the lake (Table 4). While the area gain slowed down at lake surface area stayed constant after the beginning of July, the energy input was considerable thereafter, suggesting that large amounts were transfered to the subsurface, allowing for extensive ice melt beneath the surface.

The thermokarst lake evolved over a period of 10 weeks and drained within one day through a newly formed channel, indicating that the time scale of thermokarst breakthrough is shorter than the summer season. The total amount of ice melt preceding the failure sums to ∼87,000 m^3 (corresponding energy input 2.6×10^{13} J). The impact of energy available for thermokarst evolution is emphasized by dividing this value by the distance to the debris flow initiation zone (∼350 m), and assuming a channel of circular cross section, resulting in an upper bound estimate of 18 m for the channel diameter. While only a fraction of this energy is was actually involved in channel development, the resulting order of magnitude clearly demonstrates the potential of thermokarst evolution for triggering the lake outburst during the course of a single summer season. Dividing the latest lake water volume estimate (∼166,000 m^3) by the drainage time (∼1 day) indicates a drainage rate on the order of ∼a few m^3 s^{-1}, supplying a substantial amount of water to the debris flow initiation zone. In contrast to many hazardous glacial lakes evolving over time scales of years to decades (Haeberli, 1983; Mölg et al., 2021), the thermokarst lake in Hüttekar-cirque unfolded its destructive power already two months after its formation.

6 Discussion

While the absence of instrumentation in Hüttekar-cirque during the failure inhibits a detailed reconstruction of the debris flow initiation mechanism, the relative importance of destabilizing factors can confidently be evaluated.

Unfavorable topographical and sedimentological predisposition put the rock glacier front in a state susceptible to debris flow initiation. Its steep slope angle supports shear stress and sensitivity to liquefaction while lowering shear strength (Iverson et al., 1997; Chowdhury et al., 2010; Reichenbach et al., 2018). Convex topography generally (Iverson et al., 1997). The convex top induces extensive deformation patterns favoring the development of tensional stresses (Roer et al., 2008; Delaloye et al., 2013; Marcer et al., 2019). Since the rock glacier did not show discernible signs of destabilization prior to debris flow initiation, external drivers including the strong increase in air temperature and positive degree day sum, along with available snow and ice meltwater and their pronounced impact on permafrost during the months preceding the debris flow event are considered crucial preparatory factors (Table 3)(Delaloye et al., 2013; Marcer et al., 2019). Rock glacier creep balancing erosion rates at the rock glacier front, in combination with a high energy environment favoring permafrost degradationat the rock glacier front provide , provides a large accumulation of loose, unfrozen sedimentthat is susceptible to . The eroded material is available for subsequent mobilization down the adjacent steep slope(Fig. 5, Fig. S2), inhibiting the formation of a stabilizing debris accumulation at the toe of the rock glacier front (Kummert and Delaloye, 2018).

Debris slides within saturated, loose sediment responding contractive to shear deformation are prone to mobilize into debris flows (Savage and Baum, 2005). Collapse of the soil structure and crushing of particles drives drive the development of transient excess pore-water pressures in parts of the deforming mass, which reacts by disintegration and acceleration (Hutchinson and Bhandari, 1971; Iverson and Major, 1986; Anderson and Sitar, 1995; Iverson, 1997, 2005, 1997; Sassa and Wang, 2005)(Iverson and Major, 1986; Iverson et al., 1997; Sassa and Wang, 2005). Within the displaced mass, the rates of excess pore-water pressure generation and dissipation critically depend on strain rate, bulk density, and grain size distribution (Iverson, 1997, 2005; Iverson et al., 1997). Poorly (Iverson, 1997, 2005). Once saturated, poorly sorted sand and gravel , such as the Hüttekar Rock Glacier material (Fig. 6b) , are 6) is susceptible to undrained deformation and attendant pore-water pressure coevolution, demonstrating the susceptibility . Since these features document the compositional propensity of the rock glacier front to debris flow mobilization(Iverson, 1997, 2005; Iverson et al., 1997). , the remaining issues requiring clarification concern potential sources of water capable of saturating the rock glacier front material at the initiation zone.

The relative time scales for pore space contraction and pore-water pressure diffusion govern the persistence of high pore-water pressures (Iverson, 1997; Iverson and LaHusen, 1989; Iverson et al., 1997)(Iverson and LaHusen, 1989; Iverson, 1997). The diffusion time scale of Hüttekar Rock Glacier debris is relatively short (on the order of $\sim$20 s, estimated from similar material investigated at the USGS debris flow flume, Fig. 6b6; Iverson (1997)). Sustaining pore-water pressures high enough to keep debris flow surges in motion therefore requires rapid and persistent delivery of large amounts of water (on the order of a few m^3 s^{-1}).

The hydrometeorological conditions preceding the debris flow determine the critical amount of water necessary to initiate failure (Crozier, 2010). Frequency analysis of rainfall events hitting Hüttekar-cirque indicates that the event immediately preceding the debris flow was not exceptionally severe, falling below the critical threshold for failure initiation (Fig. 8). Regarding the moderately dry hydrometeorological conditions during summer 2019(Table 3), these observations suggest that the storm immediately preceding the event fails to could not provide the large amounts of water necessary to initiate and sustain the debris flowfor several hours. Considering the coincident thermokarst lake outburst, following exceptionally warm weeks characterized by considerable energy input promoting melting processes and permafrost degradation (Table 3, Table 4), a multiple trigger mechanism is regarded plausible instead.

The key issue in terms of debris flow mechanics is the rate of water transport to the initiation zone. Field evidence suggests that water flowed concentrated along a newly formed channel network from the thermokarst lake to the rock glacier front (Fig. 4e, Fig. 4f, Fig. and 4h, Fig. S2; Supplementary Fig. S1, S3, and S4). The rapid development of this efficient drainage network was facilitated by the short timescale of advective heat transport along the meltwater channels. Driven by thermal convection, the establishment of such a channel system was possible within several weeks, despite the considerable distance of ∼350 m. The energy provided by the thermokarst lake strikingly exceeded the latent heat of fusion necessary for channel evolution. Once established, this channel network provided had the capability to transport large amounts of water from the thermokarst lake to the debris flow initiation zone within a short time. Water flow velocities along these highly permeable flow paths may reach up to several cm s^{-1} (Tenthorey, 1992; Krainer and Mostler, 2002; Buchli et al., 2013; Wagner et al., 2021b), providing sufficient water to the debris flow to keep the deforming sediment saturated. Consequently, rapid drainage emptied the lake within hours,

In contrast to many hazardous glacial lakes evolving over time scales of years to decades (Haeberli, 1983; Mölg et al., 2021), the thermokarst lake in Hüttekar-cirque unfolded its destructive power already 10 weeks after its formation. Rapid drainage emptied it without apparent prior indications of a lake outburst . With respect to GLOF hazard evaluation, the decisive factor an outburst flood. The decisive factor in terms of hazard assessment is that thermokarst development and channel breakthrough happened within an extremely short time scale (on the order of weeks), driven by the high energy input during summer 2019. In terms of mechanical properties, the ice-debris mixture composing the rock glacier represents a transitional form between the common glacier dammed and moraine dammed lakes (Clague and Evans, 1994; Huggel et al., 2004; Schaub, 2015). The Hüttekar Rock Glacier The failure mechanism involved drainage channel enlargement as well as collapse of the rock glacier front, demonstrating that thermokarst development and slope failure operated synergistically. Since their contrasting time scales (∼weeks for channel enlargement, ∼seconds to hours for rock glacier front collapse) are commonly associated with different materials (ice and debris, respectively), the integration of both mechanisms distinguishes rock glaciers from glaciers and moraines in terms of GLOF hazard assessment. The large amounts of debris provided by the rock glacier favored the evolution of the outburst flood into a debris flow.

Subsequently, the hazard cascade triggered in Hüttekar-cirque was expanded by an additional element when the displaced mass reached and blocked Radurschlbach, impounding a voluminous (∼120,000 m^3) lake that threatened a large area downstream. Acknowledging that landslide dams frequently fail within a short period (hours to months) after their formation, and that common failure mechanisms including overtopping, piping and mechanical collapse are capable of triggering severe outburst floods, prediction and instant detection of these events in remote areas is crucial for risk assessment and reduction in mountainous areas (Clague and Evans, 1994; Ermini and Casagli, 2003; Schaub, 2015).

This issue will likely gain importance as climate change alters the conditions in prospective debris flow initation zones. With respect to thermokarst evolution, the key issue is the expected increase in available melting energy that is closely linked to rising air temperatures. Previous research showed that the development of thermokarst features, including lakes and channel networks, is highly sensitive to thermal ground conditions and their response to climate change (Kääb and Haeberli, 2001). Consequently, we expect the establishment of these features in areas currently characterized by permafrost. Our study shows that such channel systems might develop within weeks, and subsequently are able to transfer large amounts of water within a short time. It is this hardly predictable short-term development of thermokarst features that challenges the evaluation of slope stability under a warming mountain climate. Once established, these channel networks are capable of rapidly concentrating water at points of converging channels. This process threatens slope stability irrespective of the specific trigger mechanisms, by adding additional weight while simultaneously decreasing shear strength (Johnson and Sitar, 1990; Chowdhury et al., 2010). Its hazardous role is underpinned by concentrated water outflow in debris flow initiation zones documented at several other rock glacier fronts (Kummert et al., 2018; Marcer et al., 2020; Kofler et al., 2021). While this study is the first one to explicitely assess its rate and magnitude in this specific context, we argue that similar processes might support localized failure mechanisms of active rock glacier fronts in a wide range of settings.

7 Conclusions

The 2019 Hüttekar debris flow impounded the main river of Radurschl Valley, threatening the downstream community and infrastructure by dam breakthrough. The Local rock glacier front failure was caused by an upstream thermokarst lake outburst and mobilized into a catastrophic debris flow displacing 40,000–50,000 m^3 sediment within several hours. Analyzing a comprehensive set of potentially destabilizing factors reveals critical combinations of environmental influences that govern multi hazard characteristics in a this complex periglacial setting. Evaluating the topographical and sedimentological context, quantifying rock glacier movement rates preceding the failure, and analyzing climate and weather signals demonstrates the capability of rapid thermokarst evolution to induce highly hazardous situations at short time scales. In combination with challenges regarding hazard detection and prediction in remote areas, this complicates integrated multi hazard assessment (Kappes et al., 2012; Gallina et al., 2016). In this context, the combination of several raster data sets comprising terrain models, satellite imagery, and gridded climate and weather variables proofed a valuable tool for assessing the individual impact of destabilizing factors in complex mountainous terrain.

The observed failure differs from rock glacier front failures documented so far. Not only the amount of rainfall, but its combination with the Rapid thermokarst lake development , and the evolution of a drainage system within the rock glacier primarily caused the debris flow. The fact that a comparable thermokarst lake had never been observed before on Hüttekar Rock Glacier, and that the outburst occurred only two months 10 weeks after its formation imply that comparable lake formation and outburst are hardly predictable. As climate change progresses, this mechanism will likely gain importance due to accelerated permafrost degradation and increased energy available for thawing, altering ground properties and increasing the likelihood of thermokarst lake formation (Kääb and Haeberli, 2001; Patton et al., 2019). Since many rock glacier fronts exhibit grain size distributions similar to the Hüttekar Rock Glacier (Johnson, 1992; Haeberli and Vonder Mühll, 1996; Arenson et al., 2002; Krainer et al., 2010, 2012), they pose widespread multi hazard elements in mountainous regions, with significantly increased risk if rivers or infrastructure pass potential runout zones of debris flows.

In combination with challenges regarding hazard detection and prediction in remote areas, this complicates integrated multi hazard assessment (Kappes et al., 2012; Gallina et al., 2016). In this context, the combination of several raster data sets comprising terrain models, satellite imagery, and gridded climate and weather variables proofed a valuable tool for assessing the individual impact of destabilizing factors in complex mountainous terrain.

The observed debris flow mechanism is the most frequent one in colluvium, which covers most of the surface in mountainous terrain (Turner, 1996). Thus, we suggest that the results obtained in this study apply not only to rock glaciers, but to a wide range of colluvium in mountainous, permafrost-affected landscapes, with accordingly wide implications. Including rapid thermokarst evolution in landslide hazard assessment gains will likely gain importance as climate change progresses, altering the boundary conditions for periglacial landslides across the European Alps and mountain ranges around the world. The developed process-based understanding of the analyzed hazard cascade including thermokarst lake outburst, rock glacier front failure, debris flow evolution, and river blockage provides an expedient tool a benchmark for multi hazard identification.

Data availability. Meteorological data sets, including the Spatiotemporal Reanalysis Dataset for Climate in Austria (SPARTACUS) and the Integrated Nowcasting through Comprehensive Analysis Dataset (INCA), are continuously updated by GeoSphere Austria and freely available from https://data.hub.zamg.ac.at/ (last access: 15 February 2023). The Government of the Province of Tyrol provides the digital terrain model, current and historical ortho-images, as well as historical maps and laserscans (freely available from https://www.data.gv.at/, https://hik.tirol.gv.at/, and https://lba.tirol.gv.at/, respectively; last access: 15 February 2023). Sentinel-2 multi-spectral satellite data are provided by Copernicus and processed by Sentinel Hub (https://www.sentinel-hub.com/, last access: 15 February 2023). The Alpine Permafrost Index Map is freely available from https://doi.pangaea.de/10.1594/PANGAEA.784450 (last access 15 February 2023). The rock glacier inventory and corresponding rock glacier catchment inventory are freely available from https://doi.pangaea.de/10.1594/PANGAEA.921629 (last access 15 February 2023). The employed software is freely available from https://sourceforge.net/projects/saga-gis/ (SAGA GIS), https://grass.osgeo.org/ (GRASS GIS), and https://cran.r-project.org/ (R). Grain size analysis results, surface velocity data, and additional photographs are provided in the Supplementary Material.

Video supplement. Video documentation of the rapidly draining thermokarst lake, recorded on 13 August 2019 11:20 by Josef Waldner, is available in the Supplementary Material.

Appendix A

Ice ablation rates m, given as ice water equivalent (m s^{-1}), are calculated using a surface energy balance approach (Cuffey and Paterson, 2010):

$$m = \frac{Q_r + Q_h + Q_e + Q_p}{\lambda_f \rho_w} \tag{A1}$$

where Q_r is net radiation (W m^{-2}), Q_h is the sensible heat flux (W m^{-2}), Q_e is the latent heat flux (W m^{-2}), Q_p is the heat flux associated with precipitation (W m^{-2}), λ_f is the latent heat of fusion (3.34 × 10^5 (J kg^{-1}), and ρ_w is the density of water (kg m^{-3}) at 273.15 K. Equation (A1) assumes the glacier surface to stay at 273.15 K and neglects transfer of heat within the glacier, both assumptions considered reasonable approximations for the ablation zones of temperate glaciers during the summer season (Hock, 2005; Cuffey and Paterson, 2010). For the operational purposes of this study, estimates of the individual energy flux contributions aim at evaluating their variation between different years rather than yielding precise absolute values. Net radiation is calculated according to (Cuffey and Paterson, 2010)Cuffey and Paterson (2010):

$$Q_r = Q_s(1-\alpha) + \epsilon_a \sigma T_a^4 - \epsilon_s \sigma T_s^4 \tag{A2}$$

where Q_s is incoming shortwave radiation (W m^{-2}), T_a is air temperature (K), T_s is surface temperature (K), α is broadband surface albedo (-), ϵ_a is atmospheric emissivity (-), ϵ_s is surface emissivity (-), and σ is the Stefan-Boltzmann constant (5.67 × 10^{-8} W m^{-2} K^{-4}). As a first approximation, $\epsilon_s \approx 0.95$ for ice and water, while $\alpha \approx 0.4$ and $\alpha \approx 0.06$ for ice and water, respectively (Cuffey and Paterson, 2010). Incoming shortwave radiation is given by the superposition of direct and diffuse radiation, accounting for cloudiness (INCA) and the shadowing effect of surrounding terrain, as well as by shortwave radiation reflected by the surrounding terrain ($\alpha \approx 0.2$, GRASS GIS 8.0, Hofierka et al. (2007)). Atmospheric emissivity is parameterized as outlined by Greuell et al. (1997) and Oerlemans (2000). Sensible and latent heat fluxes are calculated by parameterization of the respective transport processes based on turbulence similarity assuming a roughness length of 10^{-2} m (Brutsaert, 2005; Brock et al., 2006; Cuffey and Paterson, 2010). The sensible heat flux is given by:

$$Q_h = c_a \rho_a C_h u (T_a - T_s) \tag{A3}$$

where c_a is the specific heat capacity of air at constant pressure (1006 J kg^{-1} K^{-1}), C_h is the heat transfer coefficient (Stanton number) (-), u is windspeed (m s^{-1}), and ρ_a is air density (kg m^{-3}). The latent heat flux is obtained using:

$$Q_e = \lambda_v \rho_a C_e u (x_a - x_s) \tag{A4}$$

where C_e is the water vapor transfer coefficient (Dalton number) (-), x_a is the specific humidity of air (-), x_s is the specific humidity at the surface (-), and λ_v is the latent heat of vaporization (2.5 × 10^6 J kg^{-1}). The heatflux associated with precipitation is estimated assuming that the rain droplet temperature T_d approaches the near-surface air temperature:

$$Q_p = c_w \rho_w P(T_d - T_s) \qquad \text{(A5)}$$

where c_w is the specific heat capacity of water at constant pressure (4219 J kg^{-1} K^{-1}), and P is the precipitation intensity (m s^{-1}).

Glacial meltwater infiltrates directly from Glockturmferner and indirectly from Hüttekarferner into Hüttekar Rock Glacier (Fig. 3). The plausibility of the caluclated ablation rates for both glaciers is evaluated by comparing them to a set of glacier ablation rates and associated energy flux contributions across the European Alps (Table A1). The results obtained for Hüttekarferner and Glockturmferner (Table A2) fall within the range given by this sample, reflecting the northward exposition and steep slope of both glaciers by comparatively smaller total ablation rates.

Author contributions. SK, TW, KK, and GW designed the study and prepared the initial draft. Formal analysis, methodology development, data collection, and visualization were performed by SK, TW, KK, MA and MO. MA, MO and KH edited and complemented the manuscript draft. GW managed and coordinated the project, including the funding acquisition.

Competing interests. The authors declare that they have no conflict of interest.

Acknowledgements. This research was funded by the Austrian Federal Ministry of Agriculture, Regions and Tourism and the Federal Provinces of Vorarlberg, Tyrol, Salzburg, Styria and Carinthia within the DaFNE project RG-AlpCatch. We We thank Catherine Bertrand and one anomymous referee for their constructive feedback and helpful comments. We also thank Josef Waldner and Gerhard Schaffenrath for witness reports, local information, discussion, and photographs. Additional photographs and information were kindly provided by Roman Außerlechner, Thomas Figl, Werner Thöny (Geological Survey of Tyrol), Rudolf Philippitsch, Magdalena Seelig, Danny F. Minahan, Ainur Kokimova, Samuel Kainz, and Irène Apra. This research was funded by the Austrian Federal Ministry of Agriculture, Forestry, Regions, and Water Management and the Federal Provinces of Vorarlberg, Tyrol, Salzburg, Styria and Carinthia within the DaFNE project RG-AlpCatch. The authors acknowledge the financial support by the University of Graz.

Table A1. Ablation rates and energy flux contributions measured and calculated at various glaciers across the European Alps (Escher-Vetter, 1985; Greuell and Oerlemans, 1989; van de Wal et al., 1992; Greuell et al., 1995, 1997; Arnold et al., 1996; Oerlemans, 2000; Brock et al., 2000; Klok and Oerlemans, 2002; Oerlemans and Klok, 2002; Willis et al., 2002; Brock et al., 2006; Oerlemans et al., 2009). Values represent averages taken over the outlined period (altitude Alt (m a.s.l.), slope Sl (°), aspect Asp, measured ice ablation rate m (cm day^{-1}), given as water equivalent assuming an ice density of 900 kg m^{-3}, total energy flux density Q (W m^{-2}), net shortwave radiation Q_s (W m^{-2}), net longwave radiation Q_l (W m^{-2}), sensible heat flux Q_h (W m^{-2}), and latent heat flux Q_e (W m^{-2}), Austria AT, Switzerland CH). The (small) precipitation heat flux is rarely reported, thus not included.

Location	**Alt**	**Sl**	**Asp**	**Period**	m	Q	Q_s	Q_l	Q_h	Q_e
Haut Glacier d'Arolla (Pennine Alps, CH)	2,964	16	N	30 May 1990–28 August 1990	3.8	101	130	-52	26	-3
Haut Glacier d'Arolla (Pennine Alps, CH)	2,964	16	N	10 August 1993–25 August 1993	6.9	167	165	-20	10	12
Hintereisferner (Ötztal Alps, AT)	3,037	16	NE	12 July 1986–22 July 1986	5.1	210	236	-45	22	-3
Hintereisferner (Ötztal Alps, AT)	3,037	16	NE	13 July 1989–30 July 1989	7.9	158	155	-8	32	-21
Pasterze[a] (Glockner Range, AT)	2,914	16	E	18 June 1994–7 August 1994	5.9	232	194	-16	45	9
Pasterze[b] (Glockner Range, AT)	2,914	16	E	21 June 1994–12 August 1994	6.3	236	185	-17	56	12
Pasterze[c] (Glockner Range, AT)	2,914	16	E	19 June 1994–12 August 1994	6.5	242	199	-19	53	9
Pasterze[d] (Glockner Range, AT)	2,914	16	E	15 June 1994–16 August 1994	3.0	109	119	-33	20	3
Pasterze[e] (Glockner Range, AT)	2,914	16	E	15 June 1994–16 August 1994	2.0	87	109	-39	19	-2
Vadret da Morteratsch (Bernina Range, CH)	3,079	21	N	01 October 1995–30 September 1998	1.6	191	177	-25	31	8
Vadret da Morteratsch (Bernina Range, CH)	3,079	21	N	01 June 1999–31 August 1999	4.0	171	139	-17	37	12
Vadret da Morteratsch (Bernina Range, CH)	3,079	21	N	01 June 2000–31 August 2000	4.7	166	140	-27	43	10
Vadret da Morteratsch (Bernina Range, CH)	3,079	21	N	01 June 2001–31 August 2001	4.8	179	147	-29	49	12
Vadret da Morteratsch (Bernina Range, CH)	3,079	21	N	01 June 2002–31 August 2002	4.9	185	144	-22	48	15
Vadret da Morteratsch (Bernina Range, CH)	3,079	21	N	01 June 2003–31 August 2003	5.7	240	173	-24	70	21
Vadret da Morteratsch (Bernina Range, CH)	3,079	21	N	01 June 2004–31 August 2004	4.7	189	158	-24	42	13
Vadret da Morteratsch (Bernina Range, CH)	3,079	21	N	01 June 2005–31 August 2005	4.9	203	173	-23	42	11
Vadret da Morteratsch (Bernina Range, CH)	3,079	21	N	01 June 2006–31 August 2006	5.5	215	181	-23	50	7
Vernagtferner (Ötztal Alps, AT)	3,166	14	S	01 June 1982–30 September 1982	1.4	57	82	-24	38	-39

[a]weather station at 2205 m a. s. l., [b]weather station at 2310 m a. s. l., [c]weather station at 2420 m a. s. l., [d]weather station at 2945 m a. s. l., [e]weather station at 3225 m a. s. l.

References

680 Adler, C., Wester, P., Bhatt, I., Huggel, C., Insarov, G. E., Morecroft, M. D., Muccione, V., and Prakash, A.: Cross-Chapter Paper 5: Mountains, in: Climate Change 2022: Impacts, Adaptation, and Vulnerability, edited by Intergovernmental Panel on Climate Change, Cambridge University Press, 2022.

Anderson, R. S., Anderson, L. S., Armstrong, W. H., Rossi, M. W., and Crump, S. E.: Glaciation of alpine valleys: The glacier – debris-covered glacier – rock glacier continuum, Geomorphology, 311, 127–142, https://doi.org/10.1016/j.geomorph.2018.03.015, 2018.

Table A2. Ablation rates and energy flux contributions calculated in this study. Values represent averages taken over the outlined period (altitude Alt (m a.s.l.), slope Sl (°), aspect Asp, measured ice ablation rate *m* (cm day^{-1}), given as water equivalent assuming an ice density of 900 kg m^{-3}, total energy flux density Q (W m^{-2}), net shortwave radiation Q_s (W m^{-2}), net longwave radiation Q_l (W m^{-2}), sensible heat flux Q_h (W m^{-2}), and latent heat flux Q_e (W m^{-2})).

Location	**Alt**	**Sl**	**Asp**	**Period**	m	Q	Q_s	Q_l	Q_h	Q_e
Glockturmferner	2,855	27	N	01 June 2015–31 August 2015	2.5	90	84	-14	28	-8
Glockturmferner	2,855	27	N	01 June 2016–31 August 2016	2.2	77	77	-17	19	-2
Glockturmferner	2,855	27	N	01 June 2017–31 August 2017	2.5	91	78	-11	31	-7
Glockturmferner	2,855	27	N	01 June 2018–31 August 2018	2.2	79	79	-16	21	-5
Glockturmferner	2,855	27	N	01 June 2019–31 August 2019	2.6	97	82	-12	30	-3
Hüttekarferner	3,043	21	N	01 June 2015–31 August 2015	3.9	145	135	-9	32	-13
Hüttekarferner	3,043	21	N	01 June 2016–31 August 2016	3.5	127	123	-12	24	-8
Hüttekarferner	3,043	21	N	01 June 2017–31 August 2017	3.7	139	125	-6	32	-12
Hüttekarferner	3,043	21	N	01 June 2018–31 August 2018	3.6	133	127	-10	26	-10
Hüttekarferner	3,043	21	N	01 June 2019–31 August 2019	3.9	146	134	-8	27	-7

Anderson, S. A. and Sitar, N.: Analysis of Rainfall-Induced Debris Flows, Journal of Geotechnical Engineering, 121, 544–552, https://doi.org/10.1061/(ASCE)0733-9410(1995)121:7(544), 1995.

Arenson, L., Hoelzle, M., and Springman, S.: Borehole deformation measurements and internal structure of some rock glaciers in Switzerland, Permafrost and Periglacial Processes, 13, 117–135, https://doi.org/10.1002/ppp.414, 2002.

Arenson, L. U. and Springman, S. M.: Mathematical descriptions for the behaviour of ice-rich frozen soils at temperatures close to 0 °C, Canadian Geotechnical Journal, 42, 431–442, https://doi.org/10.1139/T04-109, 2005.

Arenson, L. U., Hauck, C., Hilbich, C., Seward, L., Yamato, Y., and Springman, S.: Sub-surface Heterogeneities in the Murtèl – Corvatsch Rock Glacier, Switzerland, in: Proceedings of the joint 63rd Canadian Geotechnical Conference and the 6th Canadian Permafrost Conference, edited by Canadian Geotechnical Society, pp. 1494–1500, Calgary, Alberta, 2010.

Arnold, N. S., Willis, I. C., Sharp, M. J., Richards, K. S., and Lawson, W. J.: A distributed surface energy-balance model for a small valley glacier. I. Development and testing for Haut Glacier d' Arolla, Valais, Switzerland, Journal of Glaciology, 42, 77–89, https://doi.org/10.3189/S0022143000030549, 1996.

Avian, M., Kaufmann, V., and Lieb, G. K.: Recent and Holocene dynamics of a rock glacier system: The example of Langtalkar (Central Alps, Austria), Norsk Geografisk Tidsskrift - Norwegian Journal of Geography, 59, 149–156, https://doi.org/10.1080/00291950510020637, 2007.

Avian, M., Kellerer-Pirklbauer, A., and Bauer, A.: LiDAR for monitoring mass movements in permafrost environments at the cirque Hinteres Langtal, Austria, between 2000 and 2008, Natural Hazards and Earth System Sciences, 9, 1087–1094, https://doi.org/10.5194/nhess-9-1087-2009, 2009.

Beniston, M., Farinotti, D., Stoffel, M., Andreassen, L. M., Coppola, E., Eckert, N., Fantini, A., Giacona, F., Hauck, C., Huss, M., Huwald, H., Lehning, M., López-Moreno, J.-I., Magnusson, J., Marty, C., Morán-Tejéda, E., Morin, S., Naaim, M., Provenzale, A., Rabatel, A., Six, D., Stötter, J., Strasser, U., Terzago, S., and Vincent, C.: The European mountain cryosphere: A review of its current state, trends, and future challenges, The Cryosphere, 12, 759–794, https://doi.org/10.5194/tc-12-759-2018, 2018.

Bodin, X., Krysiecki, J.-M., Schoeneich, P., Le Roux, O., Lorier, L., Echelard, T., Peyron, M., and Walpersdorf, A.: The 2006 Collapse of the Bérard Rock Glacier (Southern French Alps), Permafrost and Periglacial Processes, 28, 209–223, https://doi.org/10.1002/ppp.1887, 2017.

Boeckli, L., Brenning, A., Gruber, A., and Noetzli, J.: Alpine permafrost index map, https://doi.org/10.1594/PANGAEA.784450, supplement to: Boeckli, L et al. (2012): Permafrost distribution in the European Alps: calculation and evaluation of an index map and summary statistics. The Cryosphere, 6, 807-820, https://doi.org/10.5194/tc-6-807-2012, 2012a.

Boeckli, L., Brenning, A., Gruber, S., and Noetzli, J.: Permafrost distribution in the European Alps: Calculation and evaluation of an index map and summary statistics, The Cryosphere, 6, 807–820, https://doi.org/10.5194/tc-6-807-2012, 2012b.

Borga, M., Stoffel, M., Marchi, L., Marra, F., and Jakob, M.: Hydrogeomorphic response to extreme rainfall in headwater systems: Flash floods and debris flows, Journal of Hydrology, 518, 194–205, https://doi.org/10.1016/j.jhydrol.2014.05.022, 2014.

Bracken, L. J., Turnbull, L., Wainwright, J., and Bogaart, P.: Sediment connectivity: A framework for understanding sediment transfer at multiple scales, Earth Surface Processes and Landforms, 40, 177–188, https://doi.org/10.1002/esp.3635, 2015.

Brock, B. W., Willis, I. C., Sharp, M. J., and Arnold, N. S.: Modelling seasonal and spatial variations in the surface energy balance of Haut Glacier d'Arolla, Switzerland, Annals of Glaciology, 31, 53–62, https://doi.org/10.3189/172756400781820183, 2000.

Brock, B. W., Willis, I. C., and Sharp, M. J.: Measurement and parameterization of aerodynamic roughness length variations at Haut Glacier d'Arolla, Switzerland, Journal of Glaciology, 52, 281–297, https://doi.org/10.3189/172756506781828746, 2006.

Bronaugh, D.: PCIC Implementation of Climdex Routines: R package 'climdex.pcic', https://cran.r-project.org/web/packages/climdex.pcic/, last accessed 28 June 2022, 2020.

Brunetti, M. T., Peruccacci, S., Rossi, M., Luciani, S., Valigi, D., and Guzzetti, F.: Rainfall thresholds for the possible occurrence of landslides in Italy, Natural Hazards and Earth System Sciences, 10, 447–458, https://doi.org/10.5194/nhess-10-447-2010, 2010.

Brutsaert, W.: Hydrology: An Introduction, Cambridge University Press, Cambridge, 2005.

Buchli, T., Merz, K., Zhou, X., Kinzelbach, W., and Springman, S. M.: Characterization and Monitoring of the Furggwanghorn Rock Glacier, Turtmann Valley, Switzerland: Results from 2010 to 2012, Vadose Zone Journal, 12, https://doi.org/10.2136/vzj2012.0067, 2013.

Buchli, T., Kos, A., Limpach, P., Merz, K., Zhou, X., and Springman, S. M.: Kinematic investigations on the Furggwanghorn Rock Glacier, Switzerland, Permafrost and Periglacial Processes, 29, 3–20, https://doi.org/10.1002/ppp.1968, 2018.

Buckel, J., Otto, J. C., Prasicek, G., and Keuschnig, M.: Glacial lakes in Austria - Distribution and formation since the Little Ice Age, Global and Planetary Change, 164, 39–51, https://doi.org/10.1016/j.gloplacha.2018.03.003, 2018.

Burger, K. C., Degenhardt, J. J., and Giardino, J. R.: Engineering geomorphology of rock glaciers, Geomorphology, 31, 93–132, https://doi.org/10.1016/S0169-555X(99)00074-4, 1999.

Chowdhury, R., Bhattacharya, G., and Flentje, P.: Geotechnical slope analysis, CRC Press, Boca Raton, 2010.

Cicoira, A., Beutel, J., Faillettaz, J., and Vieli, A.: Water controls the seasonal rhythm of rock glacier flow, Earth and Planetary Science Letters, 528, 115 844, https://doi.org/10.1016/j.epsl.2019.115844, 2019.

Clague, J. J. and Evans, S. G.: Formation and failure of natural dams in the Canadian Cordillera, 1994.

Clague, J. J. and O'Connor, J. E.: Glacier-Related Outburst Floods, in: Snow and Ice-Related Hazards, Risks, and Disasters, edited by Haeberli, W., Whiteman, C., and Shroder, Jr., J. F., pp. 487–519, Elsevier, Amsterdam, 2015.

Clarke, G. K. C.: Glacier Outburst Floods From "Hazard Lake", Yukon Territory, and the Problem of Flood Magnitude Prediction, Journal of Glaciology, 28, 3–21, https://doi.org/10.3189/S0022143000011746, 1982.

Clarke, G. K. C.: Hydraulics of subglacial outburst floods: New insights from the Spring–Hutter formulation, Journal of Glaciology, 49, 299–313, https://doi.org/10.3189/172756503781830728, 2003.

Conrad, O., Bechtel, B., Bock, M., Dietrich, H., Fischer, E., Gerlitz, L., Wehberg, J., Wichmann, V., and Böhner, J.: System for Automated Geoscientific Analyses (SAGA) v. 2.1.4, Geoscientific Model Development, 8, 1991–2007, https://doi.org/10.5194/gmd-8-1991-2015, 2015.

Crameri, F.: Scientific colour maps: perceptually uniform and colour-vision deficiency friendly, https://doi.org/10.5281/zenodo.1243862, 2018.

Crozier, M. J.: Deciphering the effect of climate change on landslide activity: A review, Geomorphology, 124, 260–267, https://doi.org/10.1016/j.geomorph.2010.04.009, 2010.

Cruden, D. M. and Varnes, D. J.: Landslide Types and Processes, in: Landslides, edited by Turner, A. K. and Schuster, R. L., Transportation Research Board Special Report, pp. 36–75, National Academy of Sciences, Washington, 1996.

Cuffey, K. M. and Paterson, W. S. B.: The Physics of Glaciers, Elsevier Butterworth Heinemann, Burlington, MA, 4 edn., 2010.

Delaloye, R., Morard, S., Barboux, C., Abbet, D., Gruber, V., Riedo, M., and Gachet, S.: Rapidly moving rock glaciers in Mattertal, in: Mattertal - ein Tal in Bewegung, edited by Graf, C., pp. 21–31, Eidgenössische Forschungsanstalt für Wald, Schnee und Landschaft (WSL), Birmensdorf, 2013.

Deline, P., Gruber, S., Delaloye, R., Fischer, L., Geertsema, M., Giardino, M., Hasler, A., Kirkbride, M., Krautblatter, M., Magnin, F., McColl, S., Ravanel, L., and Schoeneich, P.: Ice Loss and Slope Stability in High-Mountain Regions, in: Snow and Ice-Related Hazards, Risks, and Disasters, edited by Haeberli, W., Whiteman, C., and Shroder, Jr., J. F., pp. 521–561, Elsevier, Amsterdam, 2015.

Destro, E., Marra, F., Nikolopoulos, E. I., Zoccatelli, D., Creutin, J. D., and Borga, M.: Spatial estimation of debris flows-triggering rainfall and its dependence on rainfall return period, Geomorphology, 278, 269–279, https://doi.org/10.1016/j.geomorph.2016.11.019, 2017.

Dowling, C. A. and Santi, P. M.: Debris flows and their toll on human life: A global analysis of debris-flow fatalities from 1950 to 2011, Natural Hazards, 71, 203–227, https://doi.org/10.1007/s11069-013-0907-4, 2014.

Duque, L. F.: Inter-Event Time Definition: R package 'IETD', https://cran.r-project.org/web/packages/IETD/, last accessed 28 June 2022, 2020.

Ermini, L. and Casagli, N.: Prediction of the behaviour of landslide dams using a geomorphological dimensionless index, Earth Surface Processes and Landforms, 28, 31–47, https://doi.org/10.1002/esp.424, 2003.

Escher-Vetter, H.: Energy Balance Calculations for the Ablation Period 1982 at Vernagtferner, Oetztal Alps, Annals of Glaciology, 6, 158–160, 1985.

Evans, S. G. and Delaney, K. B.: Catastrophic Mass Flows in the Mountain Glacial Environment, in: Snow and Ice-Related Hazards, Risks, and Disasters, edited by Haeberli, W., Whiteman, C., and Shroder, Jr., J. F., pp. 563–606, Elsevier, Amsterdam, 2015.

Fischer, A., Seiser, B., Stocker Waldhuber, M., Mitterer, C., and Abermann, J.: Tracing glacier changes in Austria from the Little Ice Age to the present using a lidar-based high-resolution glacier inventory in Austria, The Cryosphere, 9, 753–766, https://doi.org/10.5194/tc-9-753-2015, 2015.

Fleischer, F., Haas, F., Piermattei, L., Pfeiffer, M., Heckmann, T., Altmann, M., Rom, J., Stark, M., Wimmer, M. H., Pfeifer, N., and Becht, M.: Multi-decadal (1953–2017) rock glacier kinematics analysed by high-resolution topographic data in the upper Kaunertal, Austria, The Cryosphere, 15, 5345–5369, https://doi.org/10.5194/tc-15-5345-2021, 2021.

Folk, R. L. and Ward, W. C.: Brazos River bar [Texas]; a study in the significance of grain size parameters, Journal of Sedimentary Research, 27, 3–26, https://doi.org/10.1306/74D70646-2B21-11D7-8648000102C1865D, 1957.

Fox-Kemper, B., Hewitt, H. T., Xiao, C., AĐalgeirsdóttir, G., Drijfhout, S. S., Edwards, T. L., Golledge, N. R., Hemer, M., Kopp, R. E., Krinner, G., Mix, A., Notz, D., Nowicki, S., Nurhati, I. S., Ruiz, L., Sallée, J.-B., Slangen, A. B. A., and Yu, Y.: Ocean, Cryosphere and Sea Level Change., in: Climate Change 2021: The Physical Science Basis. Contribution of Working Group I to the Sixth Assessment Report of the Intergovernmental Panel on Climate Change, edited by Masson-Delmotte, V., Zhai, P., Pirani, A., Connors, S. L., Péan, C., Berger, S., Caud, N., Chen, Y., Goldfarb, L., Gomis, M. I., Huang, M., Leitzell, K., Lonnoy, E., Matthews, J. B. R., Maycock, T. K., Waterfield, T., Yelekçi, O., Yu, R., and Zhou, B., Cambridge University Press, 2021.

Freeman, T. G.: Calculating catchment area with divergent flow based on a regular grid, Computers & Geosciences, 17, 413–422, 1991.

Frei, C. and Schär, C.: A precipitation climatology of the Alps from high-resolution rain-gauge observations, International Journal of Climatology, 18, 873–900, 1998.

Gallina, V., Torresan, S., Critto, A., Sperotto, A., Glade, T., and Marcomini, A.: A review of multi-risk methodologies for natural hazards: Consequences and challenges for a climate change impact assessment, Journal of environmental management, 168, 123–132, https://doi.org/10.1016/j.jenvman.2015.11.011, 2016.

Gariano, S. L. and Guzzetti, F.: Landslides in a changing climate, Earth-Science Reviews, 162, 227–252, https://doi.org/10.1016/j.earscirev.2016.08.011, 2016.

Giardino, J. R., Vitek, J. D., and DeMorett, J. L.: A Model of Water Movement in Rock Glaciers and Associated Water Characteristics, in: Periglacial Geomorphology, edited by Dixon, J. C. and Abrahams, A. D., pp. 159–184, Wiley, Chichester, 1991.

Giorgi, F., Torma, C., Coppola, E., Ban, N., Schär, C., and Somot, S.: Enhanced summer convective rainfall at Alpine high elevations in response to climate warming, Nature Geoscience, 9, 584–589, https://doi.org/10.1038/NGEO2761, 2016.

Glade, T. and Crozier, M. J.: The Nature of Landslide Hazard Impact, in: Landslide Hazard and Risk, edited by Glade, T., Anderson, M., and Crozier, M. J., pp. 43–74, John Wiley & Sons, Chichester, 2005.

Government of the Province of Tyrol: Digital terrain model, https://www.data.gv.at/, last accessed 28 June 2022, CC-BY 4.0, 2021a.

Government of the Province of Tyrol: Current and historical orthoimagery of Tyrol, https://www.data.gv.at/, last accessed 28 June 2022, CC-BY 4.0, 2021b.

GRASS Development Team: Geographic Resources Analysis Support System (GRASS), https://grass.osgeo.org, last accessed 28 June 2022, 2022.

Greuell, W. and Oerlemans, J.: Energy Balance Calculations on and near Hintereisferner (Austria) and an Estimate of the Effect of Greenhouse Warming on Ablation, in: Glacier Fluctuations and Climatic Change, edited by Oerlemans, J., Glaciology and Quaternary Geology, pp. 305–323, Springer, Dordrecht, 1989.

Greuell, W., van den Broeke, M., Knap, W., Reijmer, C., Smeets, P., and Struijk, I.: PASTEX (PASTerze EXperiment): Field report on a glacio-meteorological experiment on the Pasterze (Austria), 1995.

Greuell, W., Knap, W. H., and Smeets, P. C.: Elevational changes in meteorological variables along a midlatitude glacier during summer, Journal of Geophysical Research, 102, 25 941–25 954, https://doi.org/10.1029/97JD02083, 1997.

Groh, T. and Blöthe, J. H.: Rock Glacier Kinematics in the Kaunertal, Ötztal Alps, Austria, Geosciences, 9, 373, https://doi.org/10.3390/geosciences9090373, 2019.

Guzzetti, F., Peruccacci, S., Rossi, M., and Stark, C. P.: Rainfall thresholds for the initiation of landslides in central and southern Europe, Meteorology and Atmospheric Physics, 98, 239–267, https://doi.org/10.1007/s00703-007-0262-7, 2007.

Haeberli, W.: Frequency and Characteristics of Glacier Floods in the Swiss Alps, Annals of Glaciology, 4, 85–90, https://doi.org/10.3189/S0260305500005280, 1983.

Haeberli, W. and Vonder Mühll, D.: On the characteristics and possible origins of ice in rock glacier permafrost, Zeitschrift für Geomorphologie, Supplementary Issues, 104, 43–57, 1996.

Haeberli, W. and Whiteman, C.: Snow and Ice-Related Hazards, Risks, and Disasters: A General Framework, in: Snow and Ice-Related Hazards, Risks, and Disasters, edited by Haeberli, W., Whiteman, C., and Shroder, Jr., J. F., pp. 1–34, Elsevier, Amsterdam, 2015.

Haeberli, W., Kääb, A., Vonder Mühll, D., and Teysseire, P.: Prevention of outburst floods from periglacial lakes at Grubengletscher, Valais, Swiss Alps, Journal of Glaciology, 47, 111–122, 2001.

Haiden, T., Kann, A., Wittmann, C., Pistotnik, G., Bica, B., and Gruber, C.: The Integrated Nowcasting through Comprehensive Analysis (INCA) System and Its Validation over the Eastern Alpine Region, Weather and Forecasting, 26, 166–183, https://doi.org/10.1175/2010WAF2222451.1, 2011.

Haque, U., Blum, P., da Silva, P. F., Andersen, P., Pilz, J., Chalov, S. R., Malet, J.-P., Auflič, M. J., Andres, N., Poyiadji, E., Lamas, P. C., Zhang, W., Peshevski, I., Pétursson, H. G., Kurt, T., Dobrev, N., García-Davalillo, J. C., Halkia, M., Ferri, S., Gaprindashvili, G., Engström, J., and Keellings, D.: Fatal landslides in Europe, Landslides, 13, 1545–1554, https://doi.org/10.1007/s10346-016-0689-3, 2016.

Haque, U., da Silva, P. F., Devoli, G., Pilz, J., Zhao, B., Khaloua, A., Wilopo, W., Andersen, P., Lu, P., Lee, J., Yamamoto, T., Keellings, D., Wu, J.-H., and Glass, G. E.: The human cost of global warming: Deadly landslides and their triggers (1995-2014), Science of the Total Environment, 682, 673–684, https://doi.org/10.1016/j.scitotenv.2019.03.415, 2019.

Hayashi, M.: Alpine Hydrogeology: The Critical Role of Groundwater in Sourcing the Headwaters of the World, Ground Water, 58, 498–510, https://doi.org/10.1111/gwat.12965, 2020.

Hiebl, J. and Frei, C.: Daily temperature grids for Austria since 1961—concept, creation and applicability, Theoretical and Applied Climatology, 124, 161–178, https://doi.org/10.1007/s00704-015-1411-4, 2016.

Hiebl, J. and Frei, C.: Daily precipitation grids for Austria since 1961—development and evaluation of a spatial dataset for hydroclimatic monitoring and modelling, Theoretical and Applied Climatology, 132, 327–345, https://doi.org/10.1007/s00704-017-2093-x, 2018.

Hirsch, R. M. and Slack, J. R.: A Nonparametric Trend Test for Seasonal Data With Serial Dependence, Water Resources Research, 20, 727–732, https://doi.org/10.1029/WR020i006p00727, 1984.

Hirsch, R. M., Slack, J. R., and Smith, R. A.: Techniques of Trend Analysis for Monthly Water Quality Data, Water Resources Research, 18, 107–121, 1982.

Hock, R.: Glacier melt: a review of processes and their modelling, Progress in Physical Geography, 29, 263–391, 2005.

Hock, R., Rasul, G., Adler, C., Cáceres, B., Gruber, S., Hirabayashi, Y., Jackson, M., Kääb, A., Kang, S., Kutuzov, S., Milner, A., Molau, U., Morin, S., Orlove, B., and Steltzer, H.: High Mountain Areas, in: IPCC Special Report on the Ocean and Cryosphere in a Changing Climate, edited by Intergovernmental Panel on Climate Change, pp. 131–202, 2019.

Hofierka, J., Suri, M., and Huld, T.: Solar irradiance and irradiation model: GRASS GIS 8.0 module ‘r.sun’, https://grass.osgeo.org/grass80/manuals/r.sun.html, last accessed 28 June 2022, 2007.

Hoinkes, G. and Thöni, M.: Evolution of the Ötztal-Stubai, Scarl-Campo and Ulten Basement Units, in: Pre-Mesozoic Geology in the Alps, edited by Raumer, J. F. and Neubauer, F., pp. 485–494, Springer Berlin Heidelberg, Berlin, Heidelberg, 1993.

Hübl, J. and Beck, M.: Ereignisdokumentation 2019, 2020.

Huggel, C., Haeberli, W., Kääb, A., Bieri, D., and Richardson, S.: An assessment procedure for glacial hazards in the Swiss Alps, Canadian Geotechnical Journal, 41, 1068–1083, https://doi.org/10.1139/t04-053, 2004.

Hungr, O.: Classification and terminology, in: Debris-flow Hazards and Related Phenomena, edited by Jakob, M. and Hungr, O., pp. 9–24, Springer-Verlag Berlin Heidelberg, 2005.

Hungr, O., Leroueil, S., and Picarelli, L.: The Varnes classification of landslide types, an update, Landslides, 11, 167–194, 2014.

Hutchinson, J. N. and Bhandari, R. K.: Undrained Loading, A Fundamental Mechanism of Mudflows and other Mass Movements, Géotechnique, 21, 353–358, https://doi.org/10.1680/geot.1971.21.4.353, 1971.

Hydrological Service of Tyrol: Hydrological summary, https://www.tirol.gv.at/umwelt/wasserwirtschaft/wasserkreislauf/hydrologische-uebersichten/, last accessed 28 June 2022, 2019.

Ikeda, A. and Matsuoka, N.: Pebbly versus bouldery rock glaciers: Morphology, structure and processes, Geomorphology, 73, 279–296, https://doi.org/10.1016/j.geomorph.2005.07.015, 2006.

Ikeda, A., Matsuoka, N., and Kääb, A.: Fast deformation of perennially frozen debris in a warm rock glacier in the Swiss Alps: An effect of liquid water, Journal of Geophysical Research, 113, https://doi.org/10.1029/2007JF000859, 2008.

International Organization for Standardization: ISO 14688-1:2017 Geotechnical investigation and testing - Identification and classification of soil - Part 1: Identification and description, 2017.

Isotta, F. A., Frei, C., Weilguni, V., Perčec Tadić, M., Lassègues, P., Rudolf, B., Pavan, V., Cacciamani, C., Antolini, G., Ratto, S. M., Munari, M., Micheletti, S., Bonati, V., Lussana, C., Ronchi, C., Panettieri, E., Marigo, G., and Vertačnik, G.: The climate of daily precipitation in the Alps: Development and analysis of a high-resolution grid dataset from pan-Alpine rain-gauge data, International Journal of Climatology, 34, 1657–1675, https://doi.org/10.1002/joc.3794, 2014.

Iverson, R. M.: The physics of debris flows, Reviews of Geophysics, 35, 245–296, 1997.

Iverson, R. M.: Debris-flow mechanics, in: Debris-flow Hazards and Related Phenomena, edited by Jakob, M. and Hungr, O., pp. 105–134, Springer-Verlag Berlin Heidelberg, 2005.

Iverson, R. M. and LaHusen, R. G.: Dynamic Pore-Pressure Fluctuations in Rapidly Shearing Granular Materials, Science, 246, 796–799, 1989.

Iverson, R. M. and Major, J. J.: Groundwater Seepage Vectors and the Potential for Hillslope Failure and Debris Flow Mobilization, Water Resources Research, 22, 1543–1548, https://doi.org/10.1029/WR022i011p01543, 1986.

Iverson, R. M., Reid, M. E., and LaHusen, R. G.: Debris-flow mobilization from landslides, Annual Review of Earth and Planetary Sciences, 25, 85–138, https://doi.org/10.1146/annurev.earth.25.1.85, 1997.

Jakob, M. and Hungr, O.: Introduction, in: Debris-flow Hazards and Related Phenomena, edited by Jakob, M. and Hungr, O., pp. 1–8, Springer-Verlag Berlin Heidelberg, 2005.

Jakob, M., Owen, T., and Simpson, T.: A regional real-time debris-flow warning system for the District of North Vancouver, Canada, Landslides, 9, 165–178, https://doi.org/10.1007/s10346-011-0282-8, 2012.

Johnson, K. A. and Sitar, N.: Hydrologic conditions leading to debris-flow initiation, Canadian Geotechnical Journal, 27, 789–801, https://doi.org/10.1139/t90-092, 1990.

Johnson, P. G.: Rock glacier types and their drainage systems, Grizzly Creek, Yukon Territory, Canadian Journal of Earth Sciences, 15, 1496–1507, 1978.

Johnson, P. G.: Micro-relief on a Rock Glacier, Dalton Range, Yukon, Canada, Permafrost and Periglacial Processes, 3, 41–47, 1992.

Jones, D. B., Harrison, S., and Anderson, K.: Mountain glacier-to-rock glacier transition, Global and Planetary Change, 181, 102 999, https://doi.org/10.1016/j.gloplacha.2019.102999, 2019a.

Jones, D. B., Harrison, S., Anderson, K., and Whalley, W. B.: Rock glaciers and mountain hydrology: A review, Earth-Science Reviews, 193, 66–90, https://doi.org/10.1016/j.earscirev.2019.04.001, 2019b.

Kääb, A. and Haeberli, W.: Evolution of a High-Mountain Thermokarst Lake in the Swiss Alps, Arctic, Antarctic, and Alpine Research, 33, 385–390, 2001.

Kääb, A., Frauenfelder, R., and Roer, I.: On the response of rockglacier creep to surface temperature increase, Global and Planetary Change, 56, 172–187, 2007.

Kainz, S.: Characterizing Groundwater Flow Dynamics and Storage Capacity in an Active Rock Glacier, Springer Fachmedien, Wiesbaden, https://doi.org/10.1007/978-3-658-37073-2, 2022.

Kappes, M. S., Keiler, M., von Elverfeldt, K., and Glade, T.: Challenges of analyzing multi-hazard risk: A review, Natural Hazards, 64, 1925–1958, https://doi.org/10.1007/s11069-012-0294-2, 2012.

Kenner, R., Pruessner, L., Beutel, J., Limpach, P., and Phillips, M.: How rock glacier hydrology, deformation velocities and ground temperatures interact: Examples from the Swiss Alps, Permafrost and Periglacial Processes, 31, 3–14, https://doi.org/10.1002/ppp.2023, 2020.

Kerschner, H.: Zeugen der Klimageschichte im oberen Radurschltal: Alte Gletscherstände und Blockgletscher in der Umgebung des Hohenzollernhauses, Zeitschrift des Deutschen und Österreichischen Alpenvereins, 107, 23–27, 1982.

Klein Tank, A. M. G., Zwiers, F. W., and Zhang, X.: Guidelines on analysis of extremes in a changing climate in support of informed decisions for adaptation, no. 72 in World Climate Data and Monitoring Programme (WCDMP), World Meteorological Organization, Geneva, 2009.

Klok, E. J. and Oerlemans, J.: Model study of the spatial distribution of the energy and mass balance of Morteratschgletscher, Switzerland, Journal of Glaciology, 48, 505–518, https://doi.org/10.3189/172756502781831133, 2002.

Knight, J., Harrison, S., and Jones, D. B.: Rock glaciers and the geomorphological evolution of deglacierizing mountains, Geomorphology, 324, 14–24, https://doi.org/10.1016/j.geomorph.2018.09.020, 2019.

Kofler, C., Mair, V., Gruber, S., Todisco, M. C., Nettleton, I., Steger, S., Zebisch, M., Schneiderbauer, S., and Comiti, F.: When do rock glacier fronts fail? Insights from two case studies in South Tyrol (Italian Alps), Earth Surface Processes and Landforms, https://doi.org/10.1002/esp.5099, 2021.

Krainer, K. and Mostler, W.: Hydrology of Active Rock Glaciers: Examples from the Austrian Alps, Arctic, Antarctic, and Alpine Research, 34, 142–149, https://doi.org/10.1080/15230430.2002.12003478, 2002.

Krainer, K. and Ribis, M.: A Rock Glacier Inventory of the Tyrolean Alps (Austria), Austrian Journal of Earth Sciences, 105, 32–47, 2012.

Krainer, K., Lang, K., and Hausmann, H.: Active Rock Glaciers at Croda Rossa/Hohe Gaisl, Eastern Dolomites (Alto Adige/South Tyrol, Northern Italy), Geogr. Fis. Dinam. Quat., pp. 25–36, 2010.

Krainer, K., Mussner, L., Behm, M., and Hausmann, H.: Multi-disciplinary investigation of an active rock glacier in the Sella Group (Dolomites; Northern Italy), Austrian Journal of Earth Sciences, 105, 48–62, 2012.

Krainer, K., Bressan, D., Dietre, B., Haas, J. N., Hajdas, I., Lang, K., Mair, V., Nickus, U., Reidl, D., Thies, H., and Tonidandel, D.: A 10,300-year-old permafrost core from the active rock glacier Lazaun, southern Ötztal Alps (South Tyrol, northern Italy), Quaternary Research, 83, 324–335, https://doi.org/10.1016/j.yqres.2014.12.005, 2015.

Kummert, M. and Delaloye, R.: Mapping and quantifying sediment transfer between the front of rapidly moving rock glaciers and torrential gullies, Geomorphology, 309, 60–76, https://doi.org/10.1016/j.geomorph.2018.02.021, 2018.

Kummert, M., Delaloye, R., and Braillard, L.: Erosion and sediment transfer processes at the front of rapidly moving rock glaciers: Systematic observations with automatic cameras in the western Swiss Alps, Permafrost and Periglacial Processes, 29, 21–33, https://doi.org/10.1002/ppp.1960, 2018.

Lugon, R. and Stoffel, M.: Rock-glacier dynamics and magnitude–frequency relations of debris flows in a high-elevation watershed: Ritigraben, Swiss Alps, Global and Planetary Change, 73, 202–210, https://doi.org/10.1016/j.gloplacha.2010.06.004, 2010.

Major, J. J.: Experimental studies of deposition by debris flows: process, characteristics of deposits, and effects of pore-fluid pressure, Dissertation, University of Washington, Seattle, 1996.

Major, J. J., Iverson, R. M., McTigue, D. F., Macias, S., and Fiedorowicz, B. K.: Geotechnical properties of debris-flow sediments and slurries, in: Debris-flow hazards mitigation: mechanics, prediction, and assessment, edited by Chen, C.-l., pp. 249–259, American Society of Civil Engineers, New York, NY, 1997.

Marcer, M., Serrano, C., Brenning, A., Bodin, X., Goetz, J., and Schoeneich, P.: Evaluating the destabilization susceptibility of active rock glaciers in the French Alps, The Cryosphere, 13, 141–155, https://doi.org/10.5194/tc-13-141-2019, 2019.

Marcer, M., Ringsø Nielsen, S., Ribeyre, C., Kummert, M., Duvillard, P.-A., Schoeneich, P., Bodin, X., and Genuite, K.: Investigating the slope failures at the Lou rock glacier front, French Alps, Permafrost and Periglacial Processes, 31, 15–30, https://doi.org/10.1002/ppp.2035, 2020.

Marcer, M., Cicoira, A., Cusicanqui, D., Bodin, X., Echelard, T., Obregon, R., and Schoeneich, P.: Rock glaciers throughout the French Alps accelerated and destabilised since 1990 as air temperatures increased, Communications Earth & Environment, 2, 383, https://doi.org/10.1038/s43247-021-00150-6, 2021.

Marchetto, A.: Mann-Kendall Test, Seasonal and Regional Kendall Tests: R package ‘rkt’, https://cran.r-project.org/web/packages/rkt/, last accessed 28 June 2022, 2021.

Marra, F.: Rainfall thresholds for landslide occurrence: Systematic underestimation using coarse temporal resolution data, Natural Hazards, 95, 883–890, https://doi.org/10.1007/s11069-018-3508-4, 2019.

Marra, F., Nikolopoulos, E. I., Creutin, J. D., and Borga, M.: Radar rainfall estimation for the identification of debris-flow occurrence thresholds, Journal of Hydrology, 519, 1607–1619, https://doi.org/10.1016/j.jhydrol.2014.09.039, 2014.

Marra, F., Nikolopoulos, E. I., Creutin, J. D., and Borga, M.: Space–time organization of debris flows-triggering rainfall and its effect on the identification of the rainfall threshold relationship, Journal of Hydrology, 541, 246–255, https://doi.org/10.1016/j.jhydrol.2015.10.010, 2016.

Matiu, M., Crespi, A., Bertoldi, G., Carmagnola, C. M., Marty, C., Morin, S., Schöner, W., Cat Berro, D., Chiogna, G., de Gregorio, L., Kotlarski, S., Majone, B., Resch, G., Terzago, S., Valt, M., Beozzo, W., Cianfarra, P., Gouttevin, I., Marcolini, G., Notarnicola, C., Petitta, M., Scherrer, S. C., Strasser, U., Winkler, M., Zebisch, M., Cicogna, A., Cremonini, R., Debernardi, A., Faletto, M., Gaddo, M., Giovannini, L., Mercalli, L., Soubeyroux, J.-M., Sušnik, A., Trenti, A., Urbani, S., and Weilguni, V.: Observed snow depth trends in the European Alps: 1971 to 2019, The Cryosphere, 15, 1343–1382, https://doi.org/10.5194/tc-15-1343-2021, 2021.

Mölg, N., Huggel, C., Herold, T., Storck, F., Allen, S., Haeberli, W., Schaub, Y., and Odermatt, D.: Inventory and evolution of glacial lakes since the Little Ice Age: Lessons from the case of Switzerland, Earth Surface Processes and Landforms, 46, 2551–2564, https://doi.org/10.1002/esp.5193, 2021.

Moser, M.: GEOFAST 1:50 000. Zusammenstellung ausgewählter Archivunterlagen der Geologischen Bundesanstalt: Blatt 172 Weißkugel, 2012.

Nikolopoulos, E. I., Crema, S., Marchi, L., Marra, F., Guzzetti, F., and Borga, M.: Impact of uncertainty in rainfall estimation on the identification of rainfall thresholds for debris flow occurrence, Geomorphology, 221, 286–297, https://doi.org/10.1016/j.geomorph.2014.06.015, 2014.

Nikolopoulos, E. I., Borga, M., Creutin, J. D., and Marra, F.: Estimation of debris flow triggering rainfall: Influence of rain gauge density and interpolation methods, Geomorphology, 243, 40–50, https://doi.org/10.1016/j.geomorph.2015.04.028, 2015a.

Nikolopoulos, E. I., Borga, M., Marra, F., Crema, S., and Marchi, L.: Debris flows in the eastern Italian Alps: Seasonality and atmospheric circulation patterns, Natural Hazards and Earth System Sciences, 15, 647–656, https://doi.org/10.5194/nhess-15-647-2015, 2015b.

Nye, J. F.: Water Flow in Glaciers: Jökulhlaups, Tunnels and Veins, Journal of Glaciology, 17, 181–207, https://doi.org/10.3189/S002214300001354X, 1976.

Oerlemans, J.: Analysis of a 3 year meteorological record from the ablation zone of Morteratschgletscher, Switzerland: Energy and mass balance, Journal of Glaciology, 46, 571–579, https://doi.org/10.3189/172756500781832657, 2000.

Oerlemans, J. and Klok, E. J.: Energy Balance of a Glacier Surface: Analysis of Automatic Weather Station Data from the Morteratschgletscher, Switzerland, Arctic, Antarctic, and Alpine Research, 34, 477–485, https://doi.org/10.1080/15230430.2002.12003519, 2002.

Oerlemans, J., Giesen, R. H., and van den Broeke, M. R.: Retreating alpine glaciers: Increased melt rates due to accumulation of dust (Vadret da Morteratsch, Switzerland), Journal of Glaciology, 55, 729–736, https://doi.org/10.3189/002214309789470969, 2009.

Olefs, M., Schöner, W., Suklitsch, M., Wittmann, C., Niedermoser, B., Neururer, A., and Wurzer, A.: SNOWGRID – A new operational snow cover model in Austria, in: Proceedings of International Snow Science Workshop, Grenoble-Chamonix, 7-11 October 2013: a merging of theory and practice, edited by Bouvet, F. N., Ruand, Y., and Lambert, R., pp. 38–45, 2013.

Olefs, M., Baumgartner, D. J., Obleitner, F., Bichler, C., Foelsche, U., Pietsch, H., Rieder, H. E., Weihs, P., Geyer, F., Haiden, T., and Schöner, W.: The Austrian radiation monitoring network ARAD – best practice and added value, Atmospheric Measurement Techniques, 9, 1513–1531, https://doi.org/10.5194/amt-9-1513-2016, 2016.

Olefs, M., Koch, R., Schöner, W., and Marke, T.: Changes in Snow Depth, Snow Cover Duration, and Potential Snowmaking Conditions in Austria, 1961–2020—A Model Based Approach, Atmosphere, 11, 1330, https://doi.org/10.3390/atmos11121330, 2020.

Pack, R. T.: Application of airborne and spaceborne remote sensing methods, in: Debris-flow Hazards and Related Phenomena, edited by Jakob, M. and Hungr, O., pp. 275–290, Springer-Verlag Berlin Heidelberg, 2005.

Patton, A. I., Rathburn, S. L., and Capps, D. M.: Landslide response to climate change in permafrost regions, Geomorphology, 340, 116–128, https://doi.org/10.1016/j.geomorph.2019.04.029, 2019.

Peruccacci, S., Brunetti, M. T., Luciani, S., Vennari, C., and Guzzetti, F.: Lithological and seasonal control on rainfall thresholds for the possible initiation of landslides in central Italy, Geomorphology, 139-140, 79–90, https://doi.org/10.1016/j.geomorph.2011.10.005, 2012.

Petley, D.: Global patterns of loss of life from landslides, Geology, 40, 927–930, https://doi.org/10.1130/G33217.1, 2012.

Potter, N.: Ice-Cored Rock Glacier, Galena Creek, Northern Absaroka Mountains, Wyoming, Geological Society of America Bulletin, 83, 3025, https://doi.org/10.1130/0016-7606(1972)83[3025:IRGGCN]2.0.CO;2, 1972.

R Core Team: R: A language and environment for statistical computing, http://www.R-project.org, last accessed 28 June 2022, 2022.

Rajczak, J. and Schär, C.: Projections of Future Precipitation Extremes Over Europe: A Multimodel Assessment of Climate Simulations, Journal of Geophysical Research: Atmospheres, 122, 10,773–10,800, https://doi.org/10.1002/2017JD027176, 2017.

Ranasinghe, R., Ruane, A. C., Vautard, R., Arnell, N., Coppola, E., Cruz, F. A., Dessai, S., Islam, A. S., Rahimi, M., Ruiz Carrascal, D., Sillmann, J., Sylla, M. B., Tebaldi, C., Wang, W., and Zaaboul, R.: Climate Change Information for Regional Impact and for Risk Assessment, in: Climate Change 2021: The Physical Science Basis. Contribution of Working Group I to the Sixth Assessment Report of the Intergovernmental Panel on Climate Change, edited by Masson-Delmotte, V., Zhai, P., Pirani, A., Connors, S. L., Péan, C., Berger, S., Caud, N., Chen, Y., Goldfarb, L., Gomis, M. I., Huang, M., Leitzell, K., Lonnoy, E., Matthews, J. B. R., Maycock, T. K., Waterfield, T., Yelekçi, O., Yu, R., and Zhou, B., Cambridge University Press, 2021.

Rebetez, M., Lugon, R., and Baeriswyl, P.-A.: Climatic change and debris flows in high mountain regions: the case study of the Ritigraben Torrent (Swiss Alps), Climatic Change, 36, 371–389, 1997.

Reichenbach, P., Rossi, M., Malamud, B. D., Mihir, M., and Guzzetti, F.: A review of statistically-based landslide susceptibility models, Earth-Science Reviews, 180, 60–91, https://doi.org/10.1016/j.earscirev.2018.03.001, 2018.

Ribis, M.: Geologisch-hydrogeologische und hydrochemische Untersuchungen in Permafrostbereichen der Ötztaler Alpen (Tirol, Österreich), Dissertation, Leopold-Franzens-Universität, Innsbruck, 2017.

Roer, I., Haeberli, W., Avian, M., Kaufmann, V., Delaloye, R., Lambiel, C., and Kääb, A.: Observations and Considerations on Destabilizing Active Rock Glaciers in the European Alps, in: Proceedings of the 9th International Conference on Permafrost, edited by Kane, D. L. and Hinkel, K. M., pp. 1505–1510, University of Alaska Fairbanks, Fairbanks, 2008.

Sassa, K. and Wang, G. h.: Mechanism of landslide-triggered debris flows: Liquefaction phenomena due to the undrained loading of torrent deposits, in: Debris-flow Hazards and Related Phenomena, edited by Jakob, M. and Hungr, O., pp. 81–104, Springer-Verlag Berlin Heidelberg, 2005.

Savage, W. and Baum, R.: Instability of steep slopes, in: Debris-flow Hazards and Related Phenomena, edited by Jakob, M. and Hungr, O., pp. 53–80, Springer-Verlag Berlin Heidelberg, 2005.

Schaub, Y.: Outburst floods from high-mountain lakes: risk analysis of cascading processes under present and future conditions, Dissertation, Universität Zürich, Zürich, 2015.

Schauwecker, S., Gascón, E., Park, S., Ruiz-Villanueva, V., Schwarb, M., Sempere-Torres, D., Stoffel, M., Vitolo, C., and Rohrer, M.: Anticipating cascading effects of extreme precipitation with pathway schemes - Three case studies from Europe, Environment international, 127, 291–304, https://doi.org/10.1016/j.envint.2019.02.072, 2019.

Scherler, M., Schneider, S., Hoelzle, M., and Hauck, C.: A two-sided approach to estimate heat transfer processes within the active layer of the Murtèl–Corvatsch rock glacier, Earth Surface Dynamics, 2, 141–154, https://doi.org/10.5194/esurf-2-141-2014, 2014.

Schlögl, M. and Matulla, C.: Potential future exposure of European land transport infrastructure to rainfall-induced landslides throughout the 21st century, Natural Hazards and Earth System Sciences, 18, 1121–1132, https://doi.org/10.5194/nhess-18-1121-2018, 2018.

Schmid, S. M., Fügenschuh, B., Kissling, E., and Schuster, R.: Tectonic map and overall architecture of the Alpine orogen, Eclogae Geologicae Helvetiae, 97, 93–117, 2004.

Sen, P. K.: Estimates of the Regression Coefficient Based on Kendall's Tau, Journal of the American Statistical Association, 63, 1379–1389, 1968.

Sentinel Hub: Modified Sentinel-2 multi-spectral satellite data, produced from European Space Agency remote sensing data provided by Copernicus, images processed by Sentinel Hub, https://www.sentinel-hub.com/, last accessed 28 June 2022, 2020.

Sidle, R. C.: Shallow groundwater fluctuations in unstable hillslopes of coastal Alaska, Zeitschrift für Gletscherkunde und Glazialgeologie, 20, 79–95, 1984.

Soeters, R. and van Westen, C. J.: Slope Instability Recognition, Analysis, and Zonation, in: Landslides, edited by Turner, A. K. and Schuster, R. L., Transportation Research Board Special Report, pp. 129–177, National Academy of Sciences, Washington, 1996.

Spring, U. and Hutter, K.: Conduit flow of a fluid through its solid phase and its application to intraglacial channel flow, Int. J. Eng. Sci., 20, 327–363, 1981a.

Spring, U. and Hutter, K.: Numerical studies of Jökulhlaups, Cold Regions Science and Technology, 4, 227–244, https://doi.org/10.1016/0165-232X(81)90006-9, 1981b.

Springman, S. M., Arenson, L. U., Yamamoto, Y., Maurer, H., Kos, A., Buchli, T., and Derungs, G.: Multidisciplinary investigations on three rock glaciers in the swiss alps: Legacies and future perspectives, Geografiska Annaler: Series A, Physical Geography, 94, 215–243, https://doi.org/10.1111/j.1468-0459.2012.00464.x, 2012.

Stoffel, M. and Huggel, C.: Effects of climate change on mass movements in mountain environments, Progress in Physical Geography, 36, 421–439, https://doi.org/10.1177/0309133312441010, 2012.

Tenthorey, G.: Perennial névés and the hydrology of rock glaciers, Permafrost and Periglacial Processes, 3, 247–252, https://doi.org/10.1002/ppp.3430030313, 1992.

Theil, H.: A rank-invariant method of linear and polynomial regression analysis, Koninklijke Nederlandse Akademie Van Wetenschappen Proceedings, 53, 386–392, 521–525, 1397–1412, 1950.

Turner, A. K.: Colluvium and Talus, in: Landslides, edited by Turner, A. K. and Schuster, R. L., Transportation Research Board Special Report, pp. 525–554, National Academy of Sciences, Washington, 1996.

van de Wal, R. S. W., Oerlemans, J., and van der Hage, J. C.: A study of ablation variations on the tongue of Hintereisferner, Austrian Alps, Journal of Glaciology, 38, 319–324, https://doi.org/10.3189/S0022143000002203, 1992.

Varnes, D. J.: Slope Movement Types and Processes, in: Landslides, edited by Schuster, R. L., Krizek, R. J., and National Research Council, Special Report, pp. 12–33, Transportation Research Board and National Academy of Sciences, Washington, D.C., 1978.

Vonder Mühll, D. S., Arenson, L. U., and Springman, S. M.: Temperature conditions in two Alpine rock glaciers, in: Proceedings of the 8th International Conference on Permafrost, edited by Phillips, M., Springman, S. M., and Arenson, L. U., pp. 1195–1200, Balkema, Lisse, 2003.

Wagner, T., Pleschberger, R., Kainz, S., Ribis, M., Kellerer-Pirklbauer, A., Krainer, K., Philippitsch, R., and Winkler, G.: The first consistent inventory of rock glaciers and their hydrological catchments of the Austrian Alps, Austrian Journal of Earth Sciences, 113, 1–23, https://doi.org/10.17738/ajes.2020.0001, 2020.

Wagner, T., Kainz, S., Helfricht, K., Fischer, A., Avian, M., Krainer, K., and Winkler, G.: Assessment of liquid and solid water storage in rock glaciers versus glacier ice in the Austrian Alps, Science of the Total Environment, 800, 149 593, https://doi.org/10.1016/j.scitotenv.2021.149593, 2021a.

Wagner, T., Kainz, S., Krainer, K., and Winkler, G.: Storage–discharge characteristics of an active rock glacier catchment in the Innere Ölgrube, Austrian Alps, Hydrological Processes, 35, 42, https://doi.org/10.1002/hyp.14210, 2021b.

Wahrhaftig, C. and Cox, A.: Rock Glaciers in the Alaska Range, Geological Society of America Bulletin, 70, 383, https://doi.org/10.1130/0016-7606(1959)70[383:RGITAR]2.0.CO;2, 1959.

Walder, J. S. and Costa, J. E.: Outburst floods from glacier-dammed lakes: The effect of mode of lake drainage on flood magnitude, Earth Surface Processes and Landforms, 21, 701–723, https://doi.org/10.1002/(SICI)1096-9837(199608)21:8<701::AID-ESP615>3.0.CO;2-2, 1996.

Werder, M. A., Bauder, A., Funk, M., and Keusen, H.-R.: Hazard assessment investigations in connection with the formation of a lake on the tongue of Unterer Grindelwaldgletscher, Bernese Alps, Switzerland, Natural Hazards and Earth System Sciences, 10, 227–237, https://doi.org/10.5194/nhess-10-227-2010, 2010.

White, S. E.: Rock Glacier Studies in the Colorado Front Range, 1961 to 1968, Arctic and Alpine Research, 3, 43–64, 1971.

Wieczorek, G. F.: Landslide Triggering Mechanisms, in: Landslides, edited by Turner, A. K. and Schuster, R. L., Transportation Research Board Special Report, pp. 76–90, National Academy of Sciences, Washington, 1996.

Wieczorek, G. F. and Glade, T.: Climatic factors influencing occurrence of debris flows, in: Debris-flow Hazards and Related Phenomena, edited by Jakob, M. and Hungr, O., pp. 325–362, Springer-Verlag Berlin Heidelberg, 2005.

Wieczorek, G. F. and Guzzetti, F.: A review of rainfall thresholds for triggering landslides, in: Mediterranean Storms, edited by European Geosciences Union, pp. 407–414, Editoriale Bios, Cosenza, Italy, 2000.

Willis, I. C., Arnold, N. S., and Brock, B. W.: Effect of snowpack removal on energy balance, melt and runoff in a small supraglacial catchment, Hydrological Processes, 16, 2721–2749, https://doi.org/10.1002/hyp.1067, 2002.

Winkler, G., Wagner, T., Krainer, K., Ribis, M., and Hergarten, S.: Hydrogeology of Rock Glaciers - Storage Capacity and Drainage Dynamics - An Overview, in: Novel methods and results of landscape research in Europe, Central Asia and Siberia, edited by Sychev, V. G. and Mueller, L., pp. 329–334, FGBNU VNII agrochimii, Moskau, 2018.

Žebre, M., Colucci, R. R., Giorgi, F., Glasser, N. F., Racoviteanu, A. E., and Del Gobbo, C.: 200 years of equilibrium-line altitude variability across the European Alps (1901−2100), Climate Dynamics, 56, 1183–1201, https://doi.org/10.1007/s00382-020-05525-7, 2021.